

UNCLASSIFIED

AD NUMBER

AD912213

LIMITATION CHANGES

TO:

Approved for public release; distribution is unlimited.

FROM:

Distribution authorized to U.S. Gov't. agencies only; Test and Evaluation; MAR 1973. Other requests shall be referred to Aviation and Surface Effects Dept., DTNSRDC, Bethesda, MD 20034.

AUTHORITY

USNSRDC ltr 24 Apr 1974

THIS PAGE IS UNCLASSIFIED



AD912213



DESIGN AND PERFORMANCE ANALYSIS OF A PROTOTYPE  
CIRCULATION CONTROL HELICOPTER ROTOR

by

Joseph B. Wilkerson

Distribution limited to U.S. Government agencies only;  
Test and Evaluation; March 1973. Other requests for  
this document must be referred to Head, Aviation and  
Surface Effects Department.



AVIATION AND SURFACE EFFECTS DEPARTMENT

Technical Note AL-290

March 1973

NAVAL  
SHIP  
RESEARCH  
AND  
DEVELOPMENT  
CENTER

BETHESDA  
MARYLAND  
20034



DESIGN AND PERFORMANCE ANALYSIS OF A PROTOTYPE  
CIRCULATION CONTROL HELICOPTER ROTOR

by

Joseph B. Wilkerson

Distribution limited to U. S. Government agencies only;  
Test and Evaluation; March 1973. Other requests for  
this document must be referred to Head, Aviation and  
Surface Effects Department (16)

March 1973

Technical Note AL-290

TABLE OF CONTENTS

	Page
SUMMARY . . . . .	1
INTRODUCTION . . . . .	2
METHODOLOGY . . . . .	3
DESIGN CONSTRAINTS . . . . .	3
DESCRIPTION OF ANALYSIS . . . . .	7
PROCEDURE . . . . .	10
DESIGN TRADE-OFF . . . . .	12
AIRFOIL GEOMETRY . . . . .	12
SLOT DESIGN . . . . .	16
SOLIDITY . . . . .	21
PERFORMANCE RESULTS . . . . .	27
EFFECT OF TIP SPEED . . . . .	27
DISC LOADING AND SOLIDITY . . . . .	29
EFFECT OF TWIST AND TAPER . . . . .	32
HOT DAY PERFORMANCE . . . . .	35
POWER COMPONENTS . . . . .	35
MASS FLOW RATES . . . . .	39
CONCLUSIONS . . . . .	44
ACKNOWLEDGEMENT . . . . .	46
APPENDIX A - BASIC SECTION DATA . . . . .	47
APPENDIX B - SECTION DATA REFINEMENTS . . . . .	50
REFERENCES . . . . .	54

LIST OF TABLES

Table 1 - Vehicle Characteristics . . . . .	4
Table 2 - Rotor Designs . . . . .	26
Table 3 - Airfoil Geometry . . . . .	26

LIST OF FIGURES

Figure 1 - Comparison of Circulation Control to Conventional Rotor Performance . . . . .	5
Figure 2 - Effects of Reduced Chord . . . . .	6
Figure 3 - Duct Flow Model and Results . . . . .	8
Figure 4 - Force Equilibrium Conditions . . . . .	10

Figure 5 - Design Procedure, Typical Hover Variations . . . . .	13
Figure 6 - Figure of Merit Variation with Root Airfoil Thickness . . . . .	14
Figure 7 - Camber Effect on Hover Figure of Merit . . . . .	15
Figure 8 - Operational Range of Section Lift Coefficient and Angle of Attack ( $C_{T/\sigma} = 0.12$ , $b = 2$ , $\theta_c = 1^\circ$ ) . .	17
Figure 9 - Typical Chordwise Pressure Distribution . . . . .	18
Figure 10 - Aft Suction Peak Locations . . . . .	19
Figure 11 - Selected Slot Location and Trailing Edge Radii . . .	20
Figure 12 - Blade Slot Height to Chord Design . . . . .	21
Figure 13 - Effect of Design Constraints . . . . .	22
Figure 14 - Figure of Merit Variation with Solidity . . . . .	23
Figure 15 - Typical Solidity Effect on Cruise Performance (Constant Section, $t/c = 0.20$ , $\delta/c = 0.0$ ) . . . . .	25
Figure 16 - Tip Speed Effect on Rotor Performance . . . . .	28
Figure 17 - Disc Loading Effect on Rotor Performance . . . . .	30
Figure 18 - Solidity Effect on Compressor Power . . . . .	31
Figure 19 - Typical Effect of Blade Twist and Taper (Constant Section, $t/c = 0.20$ , $\delta/c = 0.0$ ) . . . . .	33
Figure 20 - Effect of Twist on Cruise Efficiency . . . . .	34
Figure 21 - Hot Day Performance . . . . .	36
Figure 22 - Hover Power Components Variation with Collective Pitch . . . . .	37
Figure 23 - Typical Limits on Collective Pitch . . . . .	38
Figure 24 - Power Sensitivity to Thrust Variation . . . . .	40
Figure 25 - Power and Mass Flow Variation with Velocity . . . .	41
Figure 26 - Typical Blade Mass Flow Variation with Azimuth . . .	43
Figure A.1 - Circulation Control Airfoil Data (Ref. 5: $t/c = 0.30$ , $\lambda/c = 0.015$ , $h/c = 0.00167$ ) . .	48
Figure A.2 - Circulation Control Airfoil Data (Ref. 4: $t/c = 0.15$ , $\delta/c = 0.0$ , $h/c = 0.0013$ ) . . .	49
Figure B.1 - Section Data Camber Refinement . . . . .	51
Figure B.2 - Reynolds Number Correction . . . . .	52
Figure B.3 - Slot Height-to-Chord Refinement . . . . .	53

## SYMBOLS

A	Reference area, ft <sup>2</sup>
b	Number of blades
c	Chord length, ft
C <sub>d</sub>	Section drag coefficient
C <sub>l</sub>	Section lift coefficient
C <sub>L</sub>	Rotor lift coefficient, $L/\rho V_T^2 S$
C <sub>P</sub>	Rotor power coefficient, $P/\rho V_T^3 S$
C <sub>T</sub>	Rotor thrust coefficient, $T/\rho V_T^2 S$
C <sub>w</sub>	Mass flow coefficient $\dot{m}/\rho V_T S$
C <sub>u</sub>	Momentum coefficient, $\dot{m} V_j / qA$
D	Drag, lb
D	Diameter, ft
D <sub>e</sub>	Equivalent rotor drag, $\frac{P_T}{V_\infty} - X$ , lb
g	Gravity acceleration, 32.17 ft/sec <sup>2</sup>
H	Rotor in-plane force, lb
h	Slot height, ft
L	Rotor lift, lb
M	Mach number
$\dot{m}$	Mass flow rate, slugs/sec
P	Power, ft-lb/sec
P(*)	Blade root pressure variation, psfa
P(x)	Blade radial pressure variation, psfa
P <sub>A</sub>	Atmospheric pressure, psfa
q	Dynamic pressure, $\frac{1}{2} \rho V_\infty^2$
R	Radius, ft
R <sub>N</sub>	Reynolds number based on chord
$\bar{R}$	Gas constant, 53.3 ft <sup>3</sup> /R
r	Local blade radius, ft
r <sub>te</sub>	Airfoil trailing edge radius, ft

S	Rotor disc area, ft <sup>2</sup>
T	Rotor thrust, lb
T <sub>A</sub>	Atmospheric temperature, °R
t/c	Airfoil thickness/chord ratio
V <sub>T</sub>	Blade tip speed, ft/sec
V <sub>∞</sub>	Free stream velocity, ft/sec
V <sub>J</sub>	Jet velocity, ft/sec
W	Weight, lb
X	Rotor propulsive force, lb
x	Dimensionless radius, r/R
$\bar{x}$	Local chord station, ft
$\bar{x}/c$	Dimensionless chord

#### GREEK SYMBOLS

$\alpha$	Angle of attack, deg
$\gamma$	Ratio of specific heats, (1.4)
$\delta$	Section camber
$\eta_c$	Compressor efficiency
$\theta_c$	Collective pitch, deg
$\theta_T$	Blade twist, deg
$u$	Advance ratio, $V_\infty/V_T$
$\xi$	Dimensionless radius, r/R
$\rho$	Density, slugs/ft <sup>3</sup>
$\sigma$	Rotor solidity, $\frac{2b}{\pi} \left(\frac{c}{D}\right)_{\text{mean}}$
$\phi_i$	Induced angle, deg
$\psi$	Azimuthal angle, deg
$\Omega$	Rotational speed, rad/sec

#### Subscripts

A	Atmospheric conditions
C	Compressor
D	Duct

e	Equivalent or effective
r	Root
S	Shaft
T	Total
t	Tip
TPP	Tip path plane

## SUMMARY

A Circulation Control Rotor (CCR) has been designed for application to existing, conventional speed helicopters of the 5000 to 10000 pound weight class. A design methodology is shown which tends to minimize rotor induced power in hover while operating at near maximum airfoil section efficiency. The particular design was constrained by conventional disc loadings and blade tip speeds to be consistent with available helicopter engine/transmission combinations. The design is near optimum within these constraints and current available data. Circulation control airfoil and slot geometry design considerations are shown. Tip speed, solidity and disc loading were varied to show performance sensitivity to those parameters and to define the conditions of best overall rotor aerodynamic efficiency. The constrained CCR design was found to operate best at a thrust coefficient/solidity ratio around 0.12. At this condition hover Figure of Merit improved with increased disc loading, while cruise aerodynamic efficiency was relatively insensitive to disc loading changes. Overall performance exceeded or was equal to that of conventional rotor systems for the same weight class vehicle.

## INTRODUCTION

Research and development in Circulation Control (CC) airfoils and their application to helicopter rotors has led to a U.S. Navy program with the objective of developing a full scale flight demonstrator prototype of a Circulation Control Rotor (CCR). The initial development of efficient circulation control airfoils through analytical and experimental methods resulted in the design of a 6.7 foot diameter Higher Harmonic Circulation Control (HHCC) rotor model. The successful performance of this model and its radically simplified control system provided considerable data in both hover and forward flight. Both the HHCC rotor data and subsequent two-dimensional airfoil data have evolved a general CCR performance prediction routine which has been correlated with test results.

This study has utilized the above routine and current available data to design, within certain boundaries, a near optimum performance CCR for application to the flight demonstration program. Rotor design was constrained by existing airframe/engine availability to allow a retrofit with minimum modification. Within these constraints, several parameters were examined to establish a rotor design which would yield the best performance combination in hover and forward flight. Parameters included airfoil sections, rotor solidity, disc loading, blade twist and taper, tip speed, number of blades, and slot height considerations.

Basic differences in CC airfoil performance and that of conventional airfoils dictate that CC sections operate at higher values of  $C_L$  (around 1.4) for best efficiency. The main impact of this is to require CCR operation at higher  $C_T/\sigma$  than conventional rotor systems for comparable performance. However, existing airframe/engine combinations reflect conventional rotor disc loadings, conventional blade tip speeds, and hence conventional rotor thrust coefficients. Consequently, with these design restrictions imposed, the rotor design in this study does not reflect limits on CCR in general, but rather a near optimum design for a moderate speed retrofitted vehicle.

Several studies have been conducted, Reference 1 to 7, which describe background information and general operation of CC airfoils.

References 8 to 12 are earlier analyses of CCR performance for a selected blade configuration. The present study is a comprehensive effort to trade-off all major parameters in the design of a moderate speed, prototype CCR system. A 6.7 foot diameter model of the present rotor design is to be fabricated and evaluated.

#### METHODOLOGY

##### DESIGN CONSTRAINTS

The full scale prototype vehicle has been limited to the 5000 to 10000 pound gross weight category. A review of candidate vehicle characteristics is shown in Table 1. For any given vehicle both disc loading and tip speed are constrained by the installed power plant(s) and transmission combination. Blade radius is also constrained by main rotor to tail rotor clearance requirements. Maximum cruise velocity is limited by airframe structures and vibrations. From the above considerations a set of representative values was chosen to design around, and is identified in Table 1 as the "Design Point". Selection of such a point within a relatively narrow range of vehicles does not affect the results of comparative trade-offs (airfoil sections, twist, and taper). The quantitative non-dimensional rotor performance has been calculated over a range of disc loadings for several tip speeds which allows some scaling of performance predictions to vehicles around the "Design Point". Certainly specific rotor parameters must be used for performance calculations on a selected vehicle.

As shown in Figure 1 the CCR design must operate at higher than conventional  $C_T/\sigma$  for best hover performance. Since disc loading, tip speed, and hence  $C_T$ , are essentially fixed, solidity is the only available design parameter to yield the desired  $C_T/\sigma$ . Decreasing the blade chord to diameter ratio ( $c/D$ ) is beneficial until structural limits are reached. For given blade stiffness requirements, airfoil section thickness, and limits on materials usable modulus, there exists a lower limit on blade chord. Figure 2a shows the significant reduction in relative blade stiffness as chord is decreased. For the purposes of this study that limit was taken to be  $0.027 \leq c/D$ . This gives a minimum chord length of 0.864 ft for a typical 32 foot diameter rotor. Another

TABLE 1 - VEHICLE CHARACTERISTICS

Vehicle	OH-58	FH-1100	OH-5A	UH-2c	L-286	BO-105	Design Point
Number of Blades	2	2	4	4	4	4	?
Chord/Diameter	0.0325	0.02435	0.0214	0.0409	0.032	0.0274	?
Solidity	0.0416	0.0308	0.0545	0.104	0.0788	0.070	?
Hover Disc Loading	3.47	2.71	4.95	8.20	4.90	6.24	5.22
Tip Speed	650	650	600	660	650	670	~ 600
Hover $C_T$	0.00346	0.00271	0.00579	0.00793	0.00488	0.00583	~ 0.006
$V_{max}$ , kts	130	--	130	135	136	135	150
Fuselage D/q	6	6	5	18	8	9	8
Gross Weight	3000	2750	4700	12500	4700	5070	4200

affect of reduced chord is the associated reduction in slot height. Good CC section performance requires that the slot height-to-chord ratio ( $h/c$ ) lie within the boundaries ( $.001 \leq h/c \leq .003$ ). This indicates smaller slot heights for smaller chords, possibly creating manufacturing difficulties and fine tolerances for rotor blades of reduced chord. Naturally the problem is greatly magnified at small model scale, requiring fine craftsmanship in fabrication. Figure 2b shows slot height values versus  $c/D$  within the limits on  $h/c$  for both model scale (Dia. = 80 in) and typical full scale (Dia. = 32 ft). For comparison, the two-dimensional models of References 2 to 5 use a 0.010 inch normal slot height. Thus from both structural stiffness and slot height manufacturing considerations a very small chord is undesirable.

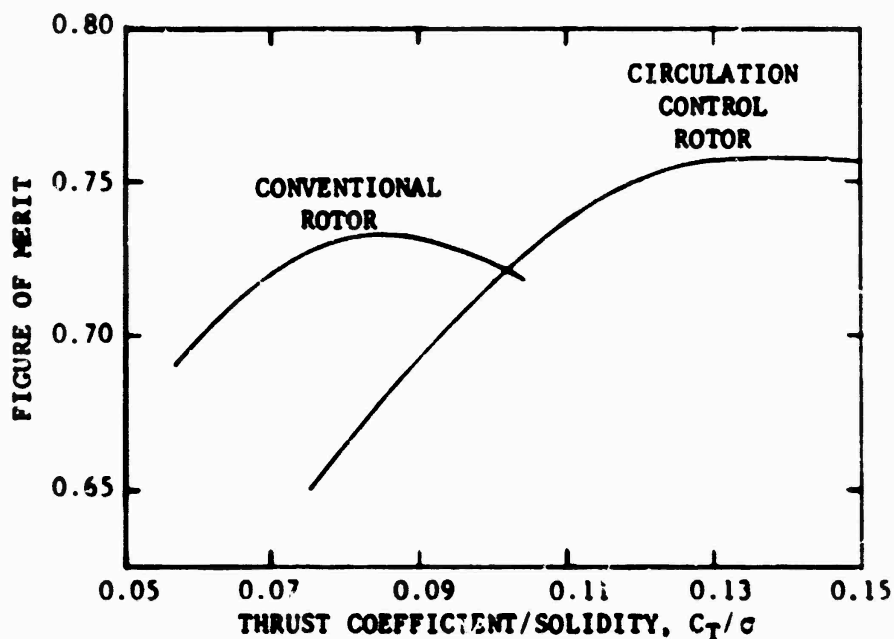


Figure 1 - Comparison of Circulation Control to Conventional Rotor Performance

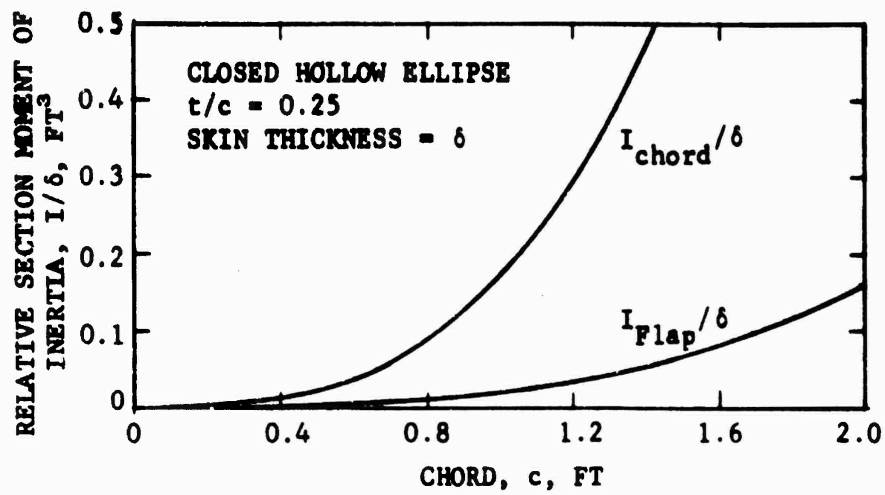


Figure 2a - Relative Stiffness Variation with Chord

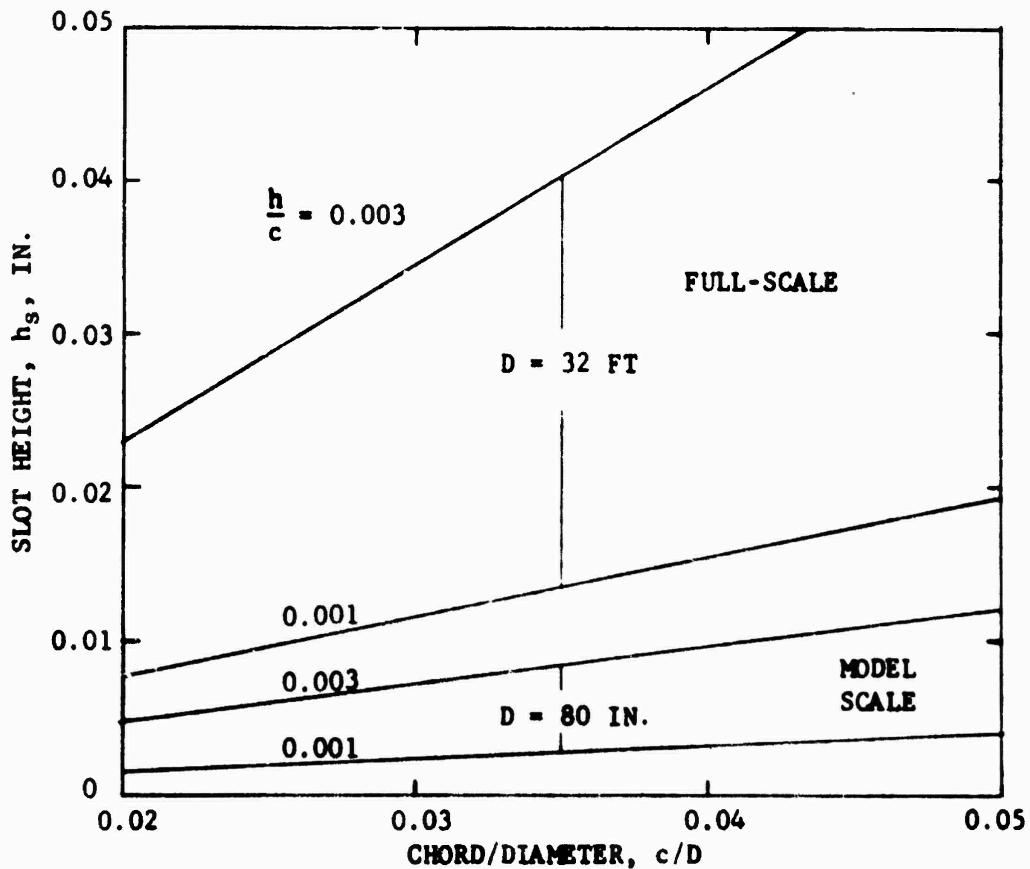


Figure 2b - Effect of Chord to Diameter Ratio on Slot Height

Figure 2 - Effects of Reduced Chord

## DESCRIPTION OF ANALYSIS

Basic CCR hover analysis techniques have been documented in Reference 10. The details of a blade duct flow analysis was also documented but was not used in the reference's rotor analysis due to cost and complexity. In lieu of that, an approximation of constant duct pressure in the radial direction was made. The present analysis does calculate variable duct pressure but by a simplified method. Results from a scaled duct flow model have shown that total pressure drop in the non-rotating duct amounts to about a 15 percent loss in relative gage pressure at the tip, with a near linear variation from root to tip, see Figure 3. The equation describing radial pressure rise due to centrifugal acceleration (for constant density) is:

$$\Delta P_{CA}(x) = \frac{1}{2} \rho_D (V_T x)^2$$

This expression added to the blade root pressure  $P(\psi)$  and applying the 15 percent loss factor gives the following description of pressure:

$$P(\psi, x) = P(\psi) - .15 [P(\psi) - P_A] x + \frac{1}{2} \rho_D (V_T x)^2 \quad (.85)$$

where  $P(\psi, x)$  and  $P(\psi)$  have dimensions of psfa. This expression may be applied to any cyclic  $P(\psi)$  variation.

Several other refinements were employed based on more detailed two-dimensional data and a correlation between performance prediction and the MHCC rotor model data. These refinements were for 1) slot height-to-chord ratio changes relative to the basic 2-D data, 2) Reynolds number correction relative to the basic 2-D data (low  $R_N$  only), 3) synthesized camber effect relative to the basic 2-D data, and 4) compressibility effects on section properties based on the results of Reference 3 (see also Reference 10). Details of the h/c refinement,  $R_N$  correction, and synthesized camber effect are given in Appendix B. The basic 2-D data curves used are given in Appendix A.

The CCR forward flight analysis includes the same corrections and 2-D data as in the hover analysis. Radial flow effects have been added to the forward flight analysis in the calculation of H-force components, although lift and torque are based on standard strip theory and do not

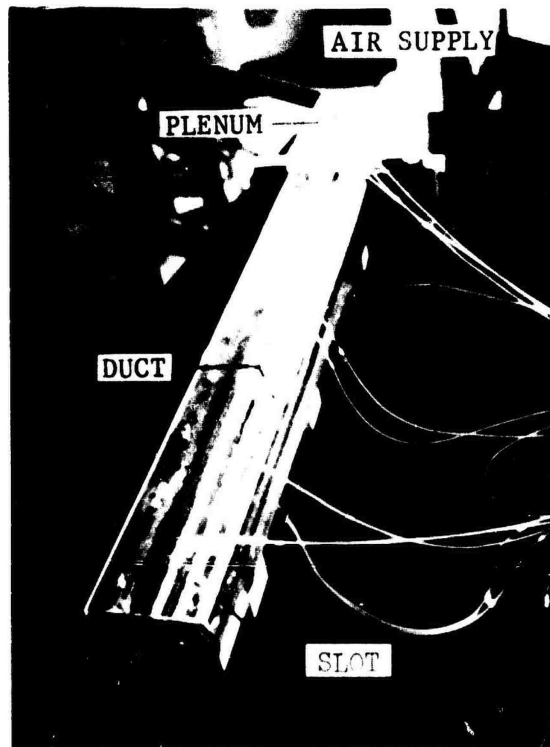


Figure 3a - Duct Flow Visualization Model

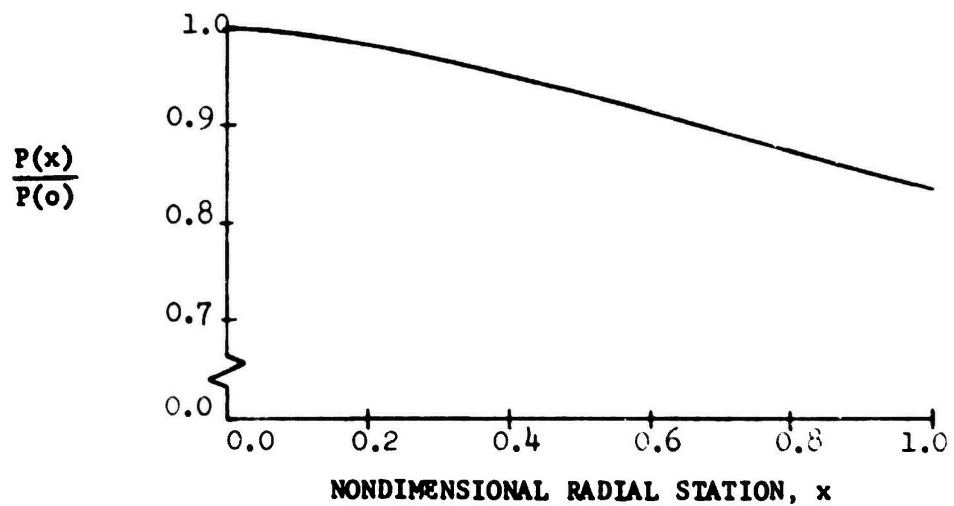


Figure 3b - Total Pressure Ratio Variation

Figure 3 - Duct Flow Model and Results

consider skewed flow. Tip assumptions do not provide lift contributing forces outboard of the 97% radial station. Profile and induced drag components at the tip are included. Rotor pitch and roll moment trims are accomplished by successive iterations on the 1/Rev cyclic blowing components, and the desired rotor thrust condition is obtained by iterations on the mean magnitude of blowing (at a specified collective pitch setting). Once the trimmed point is reached the compressor power is calculated as in the hover analysis,

$$P_c = \frac{\dot{m}_T g \bar{R} T_A \left[ \left( P_D / P_A \right)^{\frac{\gamma-1}{\gamma}} - 1 \right]}{(\gamma - 1) \eta_c}$$

where  $\eta_c = 0.8$  (compressor efficiency). Individual blade root pressure,  $P_D$ , is a function of azimuth angle in forward flight, but the peak pressure required must be maintained constantly. Therefore, this peak value of  $P_D$  is used in the above equation, along with total required rotor mass flow ( $\dot{m}_T$ ), in the calculation of compressor power ( $P_c$ ). Note that the total mass flow rate,  $\dot{m}_T$ , is really the integral of  $d\dot{m}/d\psi$ , and that only the peak point in this variation requires or uses the peak pressure mentioned above. The alternative would be to calculate  $P_c$  as a function of azimuth, using  $\dot{m}$  and  $P_D$  values appropriate to each azimuth station, and then integrate the resulting variation of  $dP_c/d\psi$ . This alternative approach would predict significantly less power required, but it is not felt to be representative of a practical control/compressor system.

The forward flight computer analysis was set to automatically increment translational velocity in steps. At each velocity the tip path plane angle was iteratively adjusted to provide equilibrium flight conditions based on input vehicle  $D/q$  and calculated rotor inplane  $H$ -force. All forward flight data presented in this report reflect the force equilibrium, moment trimmed condition for an initial vehicle disc loading in hover. Satisfying the following equations provided the simplified equilibrium condition shown in Figure 4.

$$D = \left(\frac{D}{C}\right) \frac{1}{2} \rho V_{\infty}^2$$

W = constant weight based on selected disc loading

$$T \cos \alpha_{\text{TPP}} + H \sin \alpha_{\text{TPP}} - W = 0$$

$$T \sin \alpha_{\text{TPP}} - H \cos \alpha_{\text{TPP}} - D = 0$$

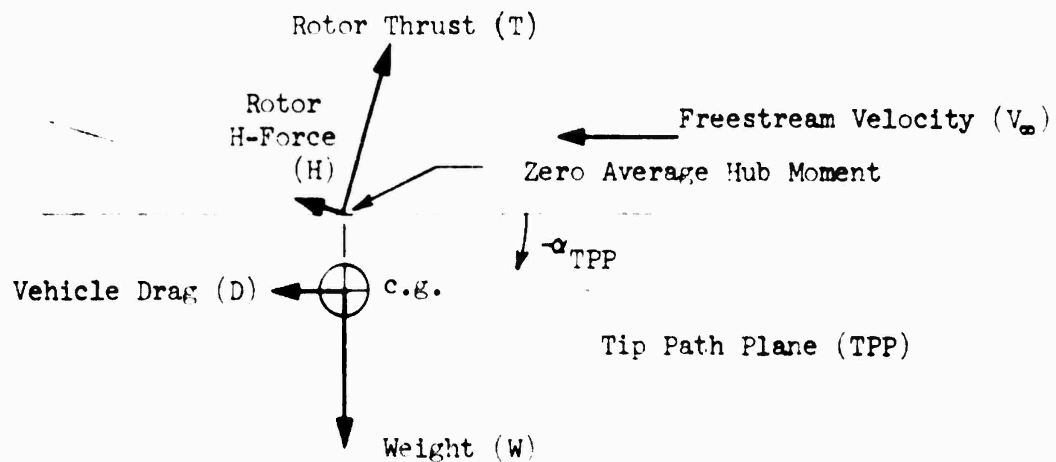


Figure 4 - Force Equilibrium Conditions

#### PROCEDURE

The additional independent variable of momentum coefficient,  $C_{\mu}$ , to describe lift distribution allows more freedom of design for a CCR than for rotors of conventional airfoil sections. Since  $C_{\mu}$  is now a function of two independent variables,  $C_{\mu}$  and  $\alpha$ , it becomes important to design the radial distribution of  $C_{\mu}$  as well as  $\alpha$ . In fact, this additional variable allows a near optimum section performance and a reduction of induced power. This radial variation of  $C_{\mu}$  was produced by a radial variation of slot opening. That is for a given radial variation of blade

duct pressure and corresponding radial variation of slot exit velocity, the mass flow rate at any radial position is determined by the slot height at that position. Another approach might be to design various internal restrictors or orifices so as to regulate the slot pressure for a finite number of radial blade segments.

The general procedure was to design slot height variation, and other parameters, for best hover performance. This was done for several rotor configurations composed of different airfoil distributions. Each rotor configuration was then evaluated for forward flight performance and the airfoil sections which produced best overall performances were determined. Three twist angles, and associated slot height variations to produce near uniform downwash at the disc in hover, were examined for each contending rotor configuration. The slot distribution and slot height were perturbed in forward flight for the better rotor designs to evaluate performance sensitivity to those parameters.

The criterion for the radial variation of slot height was to produce near uniform induced velocity at the disc in hover, thereby minimizing induced power. Uniform inflow was related to induced angle,  $\phi_1$ , through strip momentum theory relations. Lock-Goldstein hover analysis from Reference 13 then provided a target distribution of  $(\frac{C}{D}) C_{\ell}$  associated with the  $\phi_1$  above. Characteristics of the airfoil sections gave the desired radial combinations of  $C_{\ell}$  and  $\alpha$  for best section  $l/d_e$ . Specification of  $C_{\ell}$  and  $\alpha$  at two radial stations then prescribe a linear twist, linear taper, and collective pitch in conjunction with the target distributions of  $(\frac{C}{D}) C_{\ell}$  and  $\phi$ . Operating  $C_{\ell}$  and  $\alpha$  combinations for the rest of the radial positions were then calculated. The  $C_{\ell}$  needed to produce the desired  $C_{\ell}$ , at its associated  $\alpha$ , was calculated from the two-dimensional characteristics at each station. For a known internal duct pressure variation, slot exit velocity, local freestream velocity, and relative chord, a relative slot height variation may be determined which will produce the desired  $C_{\ell}$  variation. The equation describing this relative slot height distribution, based on the slot height at some radial station  $g$ , is given below:

$$\frac{h(x)}{h(\xi)} = \frac{C_{\mu}(x)}{C_{\mu}(\xi)} \frac{c/D(x)}{c/D(\xi)} \left(\frac{x}{\xi}\right)^a \left[ \frac{\left(\frac{P(\xi)}{P_A}\right)^{.286} - 1}{\left(\frac{P(x)}{P_A}\right)^{.286} - 1} \right]$$

Once the distribution is obtained it is normalized for use in performance prediction. These distributions are shown in Figure 5 along with comparative variations from performance theory which are based on the approximated slot height distribution. The above procedure has been programmed for quick calculation using a backwards table look-up to determine  $C_{\mu}$  for a given  $C_l, \alpha$  combination. The result of this procedure is a blade designed for minimum induced power in hover, with at least two radial stations operating at maximum section  $l/d_e$ , thereby reducing the profile, compressor and coriolis power components.

Non-tapered blades, or non-optimum taper, will allow only one radial station to operate at best  $l/d_e$ . This station was, of course, selected at an outboard position. For one selected  $C_l, \alpha$  point, the target  $\left(\frac{C}{D}\right) C_l$  variation and pre-determined taper prescribe all other values of relative chord and  $C_l$ . In this case a midspan station's  $C_l$  was chosen from the fixed variation. The  $\alpha$  was selected from 2-D data which gave best section  $l/d_e$  at that midspan operating  $C_l$  value. A desirable linear twist was then defined and the design proceeded, as for the optimum taper case, to determine required  $C_{\mu}$  and relative slot height variations. Note that the above values of  $C_{\mu}$  were used only for determination of relative slot height variation. They were not used directly in performance prediction.

#### DESIGN TRADE-OFF

##### AIRFOIL GEOMETRY

Initial airfoil trade-off studies were to establish the best root section geometry. Tip airfoil thickness ratio ( $t/c$ ) was established at close to 0.15 from critical Mach number considerations, with the possibility of including a small amount of camber (see Reference 7). Typical hover performance sensitivity to root section  $t/c$  is shown in Figure 6. This indicates some improvement in Figure of Merit with

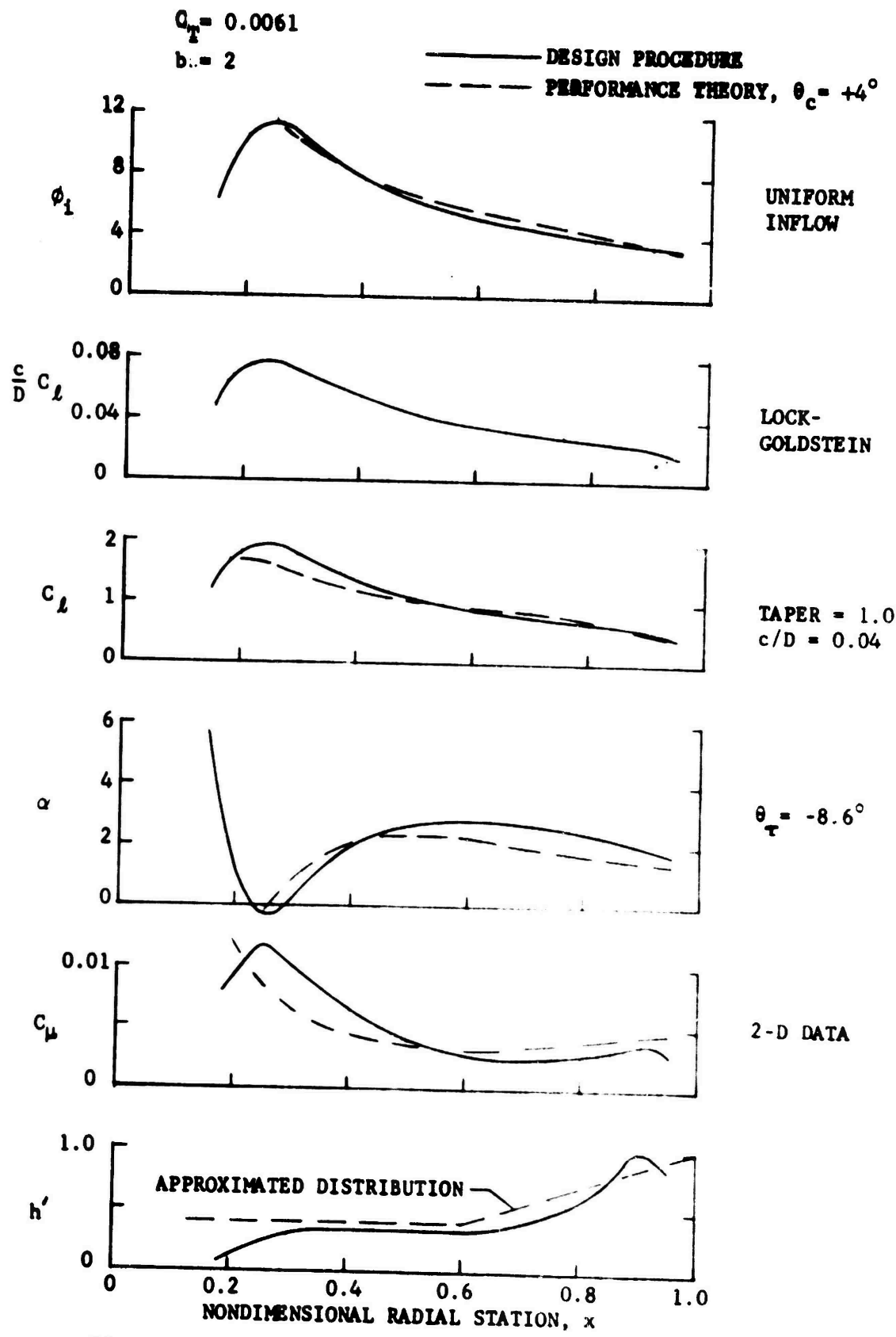


Figure 5 - Design Procedure, Typical Hover Variations

with decreasing root thickness. However, the larger thickness ellipses have larger leading edge radii which are operational over a larger angle of attack range, have larger  $C_{l_{max}}$  capability, and have generally higher augmentation. Furthermore the 20% thickness ratio cambered ellipse shows much greater efficiency, making it a desirable outboard section. Thus the root section was chosen to be 25% thick, with the 15% thick tip section, placing the more efficient 20% section near blade midspan.

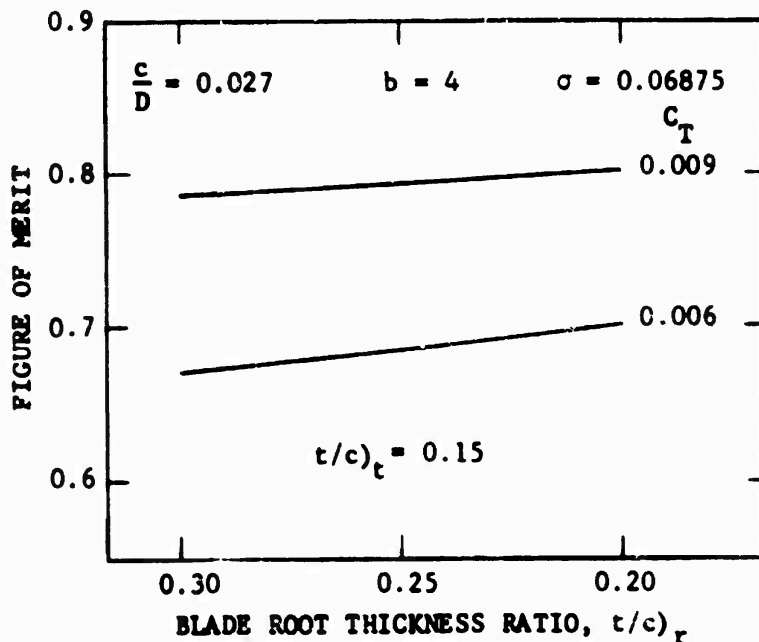


Figure 6 - Figure of Merit Variation with Root Airfoil Thickness

The effect of camber variation on rotor Figure of Merit is shown in Figure 7 for selected airfoils. This shows zero camber at the tip to be the best. An examination of blade radial distributions of  $C_l$  and  $\sigma$  clearly provide the reason. Uniform inflow dictates the desirable  $C_l, \sigma$  variation shown in Figure 5 for the design twist and constrained rotor  $C_T$ . Blade tip lift coefficients required are quite small for CC sections, and require only a small amount of blowing. The added  $\Delta C_l$  due to camber demands that

the airfoil operate at reduced angle of attack to produce the same  $C_l$ . In other words, lift due to camber at the tip cannot be efficiently utilized. Its affect must be cancelled by operation at reduced alpha which results in higher section drag and general performance reduction. This affect diminishes as thrust coefficient is increased and higher tip lift coefficients are required. The lift due to camber then becomes beneficial as seen in Figure 7 for  $C_T \geq 0.010$ . However, for a constrained rotor design ( $C_T \approx .006$ ,  $\frac{c}{D} \geq .027$ ), zero tip camber gives the better performance.

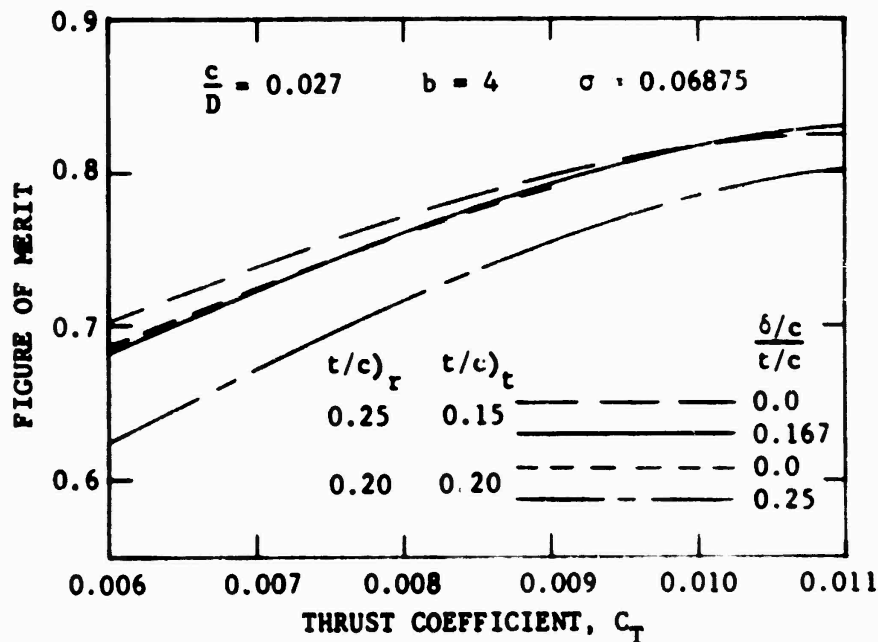


Figure 7 - Camber Effect on Hover Figure of Merit

The contrary is true for a blade root section. Relatively high  $C_l$  performance is enhanced by the addition of camber, requiring less compressor power. It also provides a more uniform chordwise pressure distribution on the airfoil. This reduces the possibility of flow separation by minimizing pressure suction peaks and the extent of adverse

pressure gradients. The maximum circular arc camber ( $\frac{\delta}{c}$ ) for an elliptical airfoil is presently considered to be one-quarter ( $1/4$ ) of the ellipse thickness ratio. This gives a nearly flat airfoil lower surface for a large percent of chord. The airfoil of Reference 2 is of such a design, and yields excellent performance. This maximum camber was utilized for the blade root airfoil, ( $t/c = .25$ ,  $\delta/c = .0625$ ). A linear variation of  $t/c$  and  $\delta/c$  from root to tip defines the included airfoil geometries.

#### SLOT DESIGN

Slot geometry design for a CC section must consider several parameters; slot height-to-chord ratio ( $h/c$ ), slot height-to-local radius ratio ( $h/r_{te}$ ), trailing edge radius-to-chord ratio ( $r_{te}/c$ ), and slot chordwise position ( $x/c$ ). The slot chordwise location must be designed to ensure attached flow in all section operating conditions including forward flight, whereas radial slot height distribution is designed for minimum induced power in hover. Design of the slot chordwise location, outlined below, is based on the procedures used in Reference 14. The significant differences are (1) the method of obtaining airfoil section operational requirements, and (2) that the procedure is applied to several sections simultaneously with consideration being given to interaction and continuity of geometry. The detailed slot design is primarily based on the chordwise location of the aft suction peak in the section pressure distribution. An operational range of  $C_l$  versus  $\alpha$  in forward flight is defined by the rotor performance prediction program for each of several radial blade sections as seen in Figure 8. When compared to a conventional airfoil  $C_l$ ,  $\alpha$  curve, this figure graphically portrays the significant difference between CCR section operation and that of conventional rotor sections. Potential flow plots are generated for boundary conditions of the operational range for each chosen blade section. A typical chordwise pressure distribution is shown in Figure 9. The suction peak locations are then defined from these pressure distributions. Since the suction peak location is dependent on trailing edge geometry (i.e., trailing edge radius), several radii were examined. The results, shown in Figure 10, typically provide a band of suction peak locations

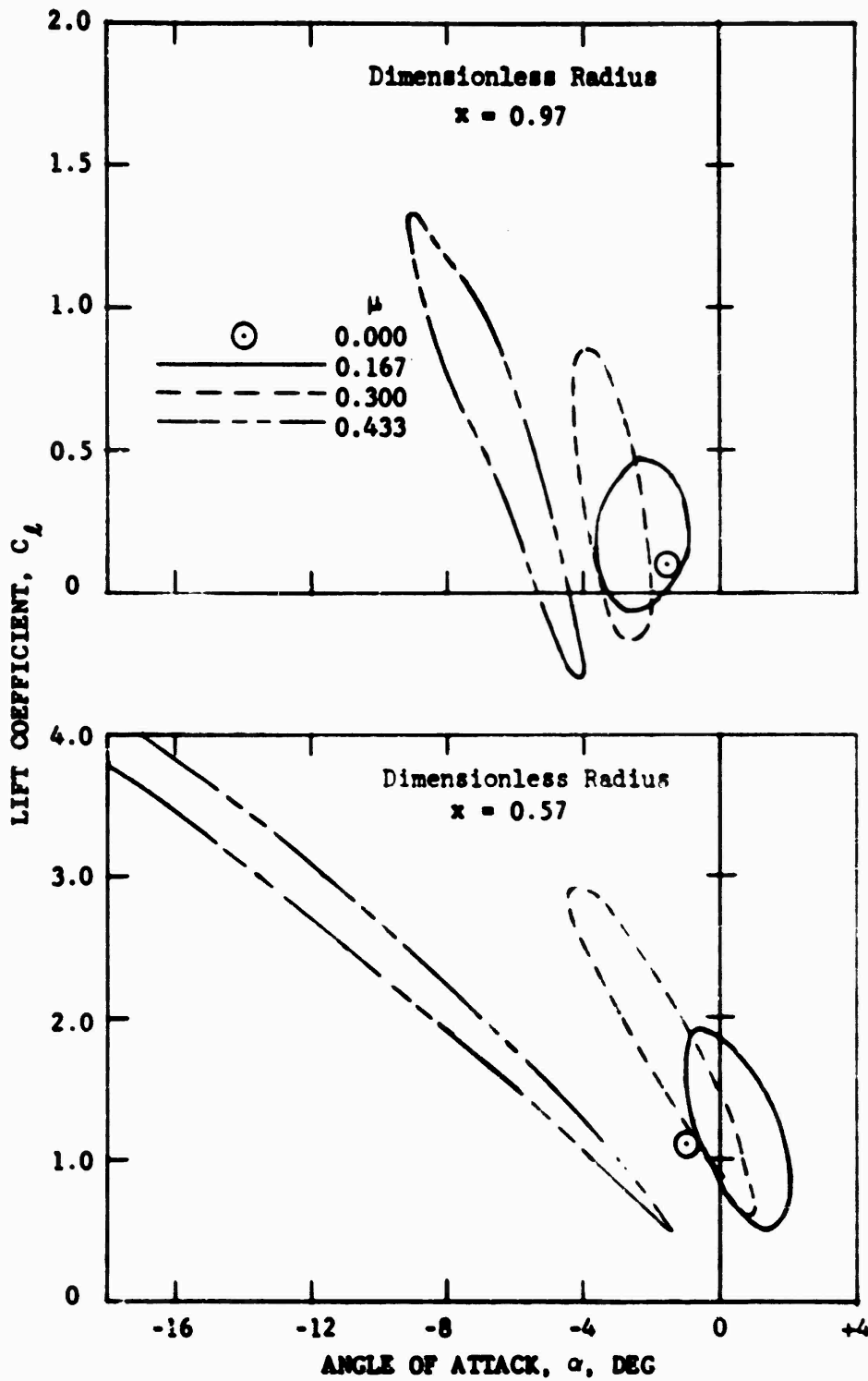
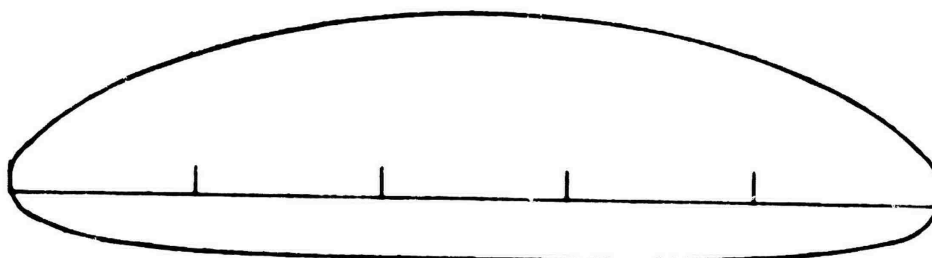


Figure 8 - Operational Range of Section Lift Coefficient and Angle of Attack ( $C_T/\sigma = 0.12$ ,  $b = 2$ ,  $\theta_c = -1^\circ$ )

THICKNESS RATIO = 0.25  
CAMBER/CHORD = 0.0625  
TRAILING EDGE RADIUS/CHORD = 0.05



ANGLE OF ATTACK = - 10.0°  
LIFT COEFFICIENT = 2.5

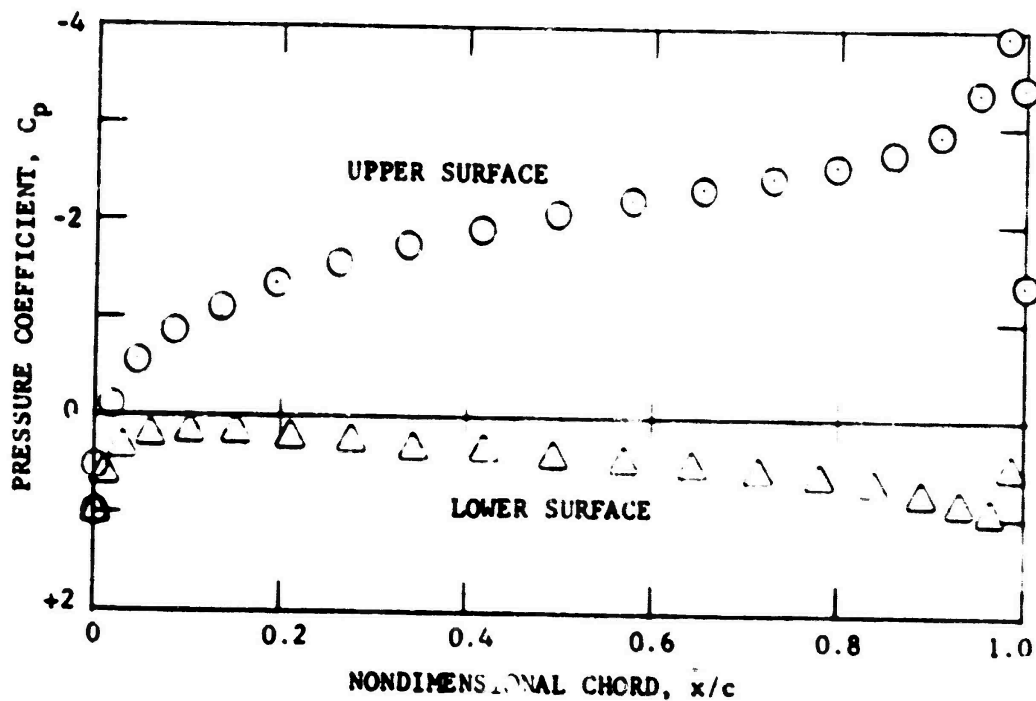


Figure 9 - Typical Chordwise Pressure Distribution

over the range of radii. The combination of airfoil trailing edge radius and chordwise location for the slot, as chosen from the above, is shown in Figure 11 (assuming a continuous circular arc also forms part of the slot).

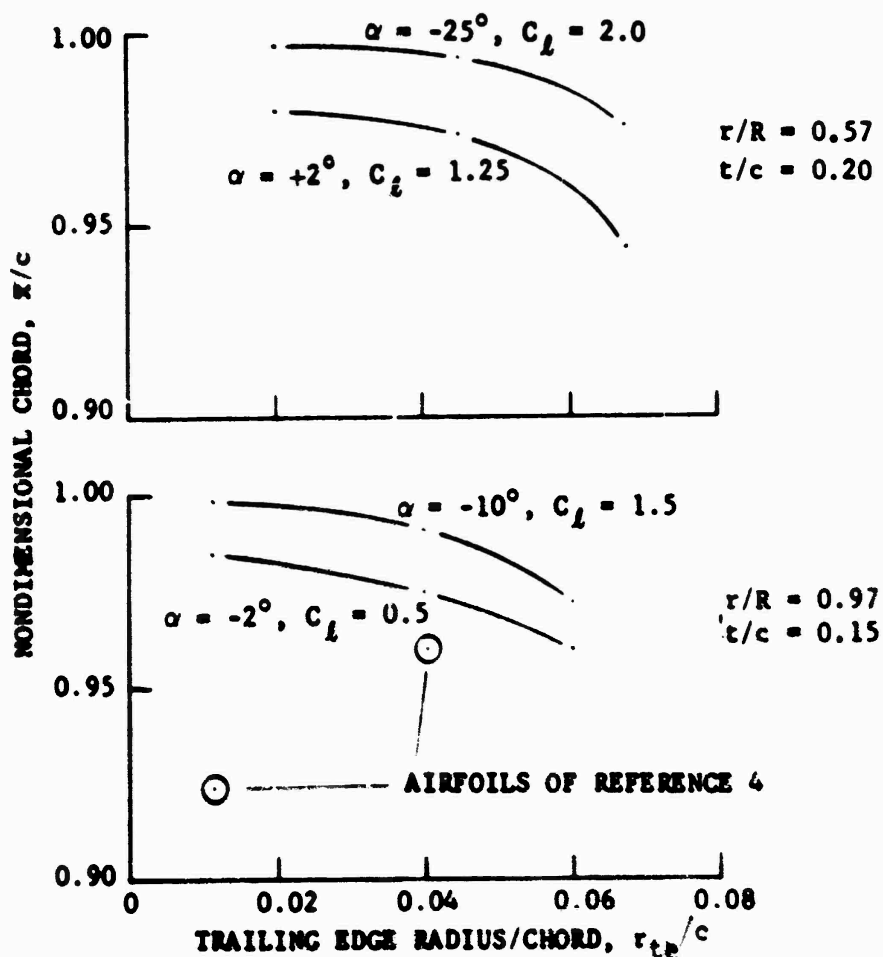


Figure 10 - Aft Suction Peak Locations

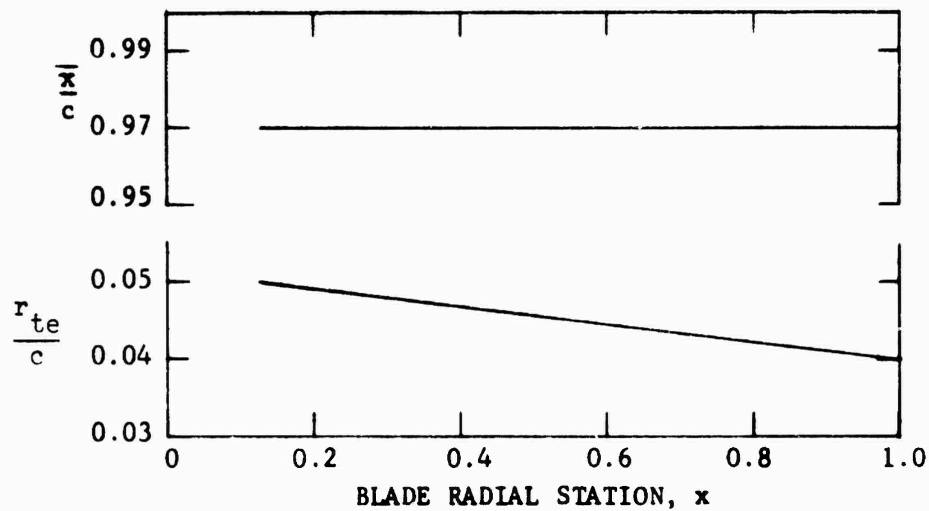


Figure 11 - Selected Slot Location and Trailing Edge Radii

The relative slot height distribution was determined from the rotor hover performance considerations, as previously described, and was shown in Figure 5. Quantitative slot height distribution was determined from (1) the relative distribution, (2) the constraints on slot height-to-chord and slot height-to-radius, and (3) the above distribution of radius-to-chord. A graph of these parameters is shown in Figure 12a and the radial variation of slot height-to-chord is shown in Figure 12b. Note that the slot distribution of Figure 5 was related only to unity, whereas the distribution of Figure 12b has been related to chord length.

Airfoil section geometry has now been defined for the blade relative to the chord ( $t/c$ ,  $\delta/c$ ,  $r_{te}/c$ ,  $\bar{x}/c$ ,  $h/c$ ). These distributions were used in succeeding performance predictions, including their impact on the refinements in Appendix B. The chord-to-diameter ratio ( $c/D$ ), or rotor solidity, was examined next.

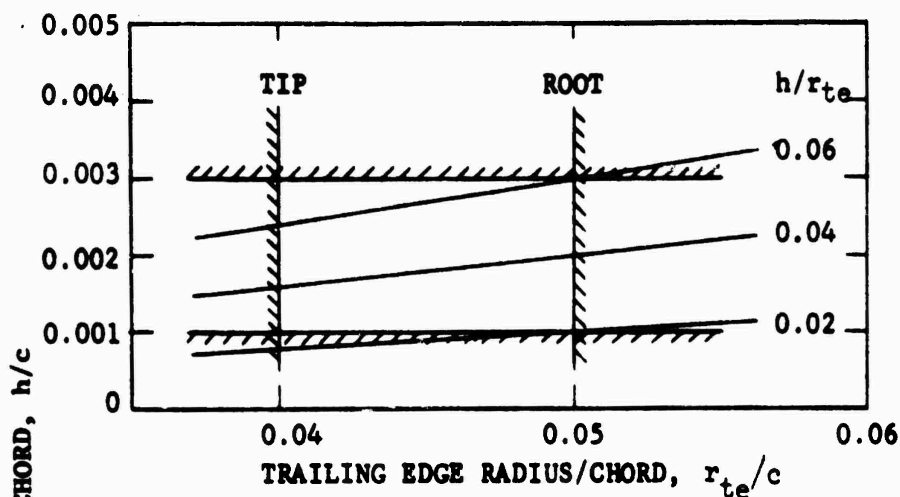


Figure 12a - Slot Height Design Constraints

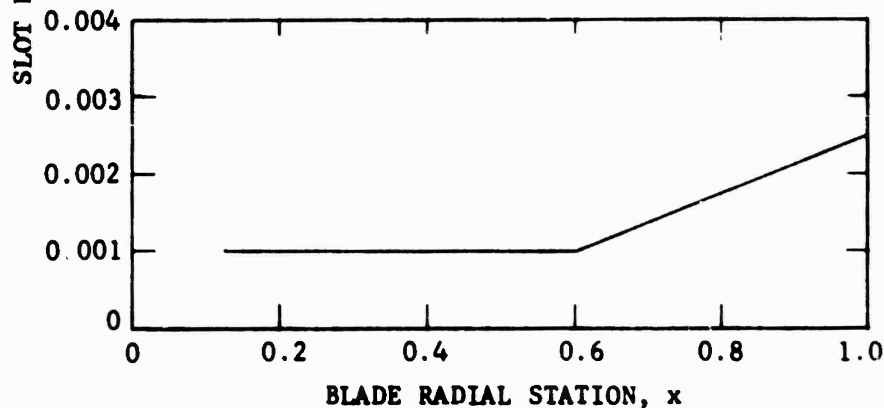


Figure 12b - Selected Slot Height/Chord Variation

Figure 12 - Blade Slot Height to Chord Design

#### SOLIDITY

Rotor solidity was previously concluded to be the least constrained design parameter to obtain a  $C_T/\sigma$  which is compatible with good CCR performance, see Figure 1. A range of solidity, associated with the desired operative range of  $C_T/\sigma$  for a specified thrust coefficient, is shown in Figure 13a for the "Design Point" of Table 1 ( $C_T = .0061$ ) and for 150% of that value ( $C_T = .009$ ). The larger  $C_T$  may be obtainable by acceptable design changes in disc loading and tip speed for some vehicles. However, for the Design Point a very low range of solidity is required.

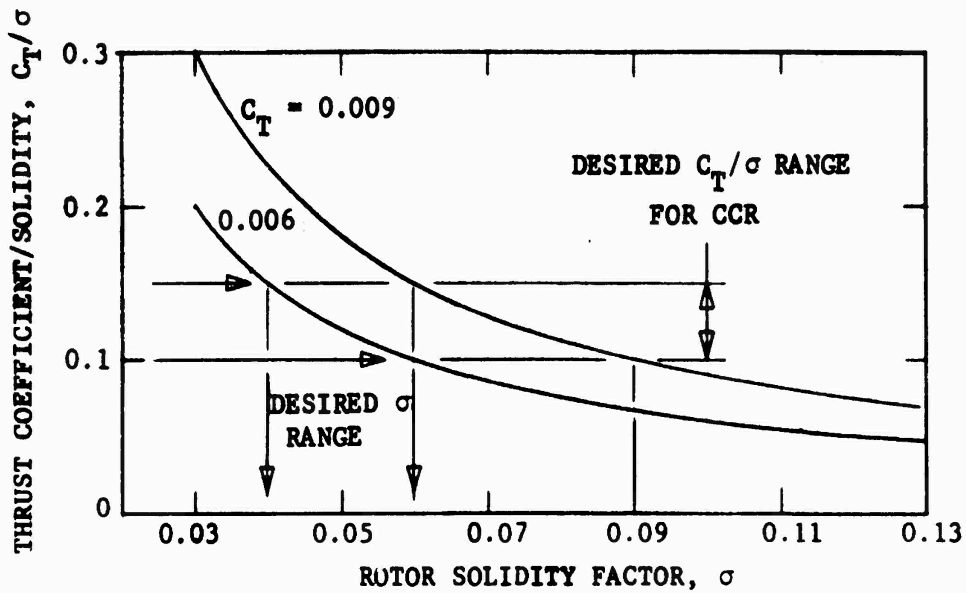


Figure 13a - Desired Rotor Solidity Range

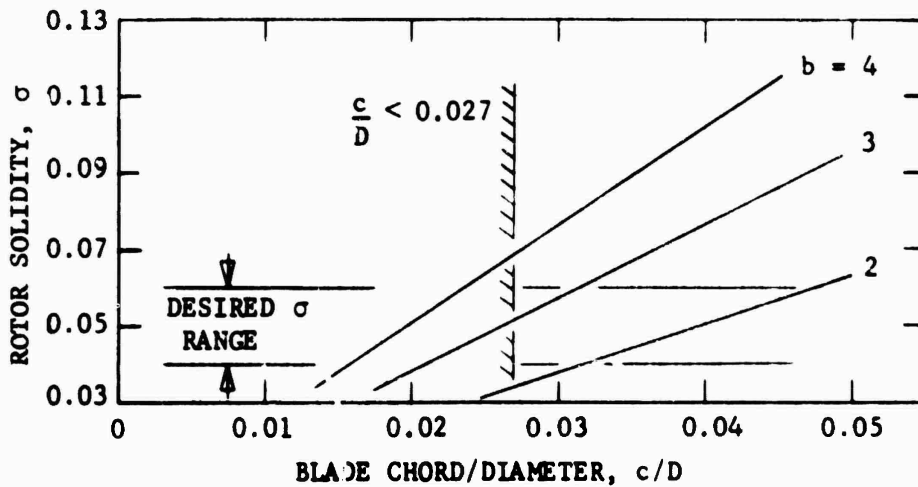


Figure 13b - Solidity Impact on Number of Blades

Figure 13 - Effect of Design Constraints

Figure 13b shows the trade-off between blade  $c/D$  and number of blades, with the constraint  $c/D \geq 0.027$  as previously discussed. These figures show maximum design  $C_T/\sigma = 0.0873$  for the four bladed rotor, which is relatively low for a CCR design even considering the cruise flight performance compromise. A two bladed rotor is seen to allow good hover performance, and at a more desirable  $c/D$  value, (see also Figure 2). The importance of lower solidity and/or higher  $C_T$  in hover is shown in Figure 14. The lowest solidity for a given number of blades is again shown in this figure, pointing up the hover performance advantage of the two or three bladed configurations. Not shown is the fact that near optimum hover performance impacts on cruise performance. The section that produces  $C_l \approx 1$  in hover may be asked to produce up to  $C_l \approx 5$  on the retreating blade at a reasonable advance ratio. This magnitude approaches the limit of even a circulation control airfoil, and is definitely not an efficient operating condition.

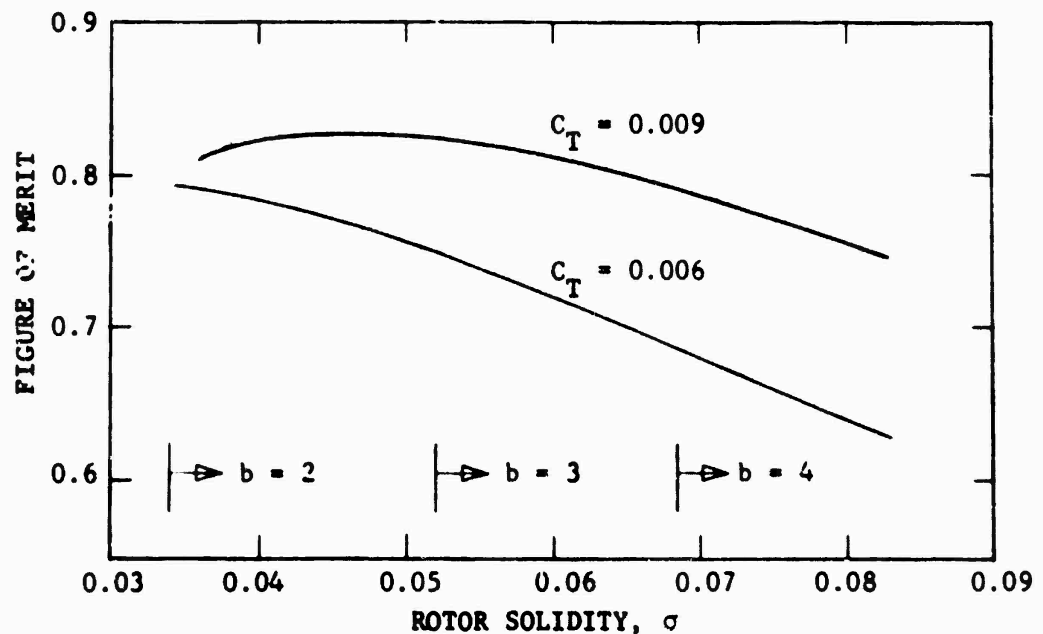


Figure 14 - Figure of Merit Variation with Solidity

The trade-off between hover and forward flight performance was examined for a two bladed rotor and a four bladed rotor. The performance comparison was based on rotor lift to equivalent drag ratio ( $L/D_e$ ). Four solidities were considered for each number of blades to allow a sufficient range. Typical results are shown in Figure 15 for one of the airfoil selections ( $t/c = 0.20$ ,  $\delta/c = 0.00$ , constant section). This shows that performance of the four bladed rotor continually improves with decreasing  $c/D$ , even until the lowest  $c/D$  begins to pay a penalty at the higher speeds. Rotor  $C_T/\sigma$  was raised still further by decreasing  $c/D$  for the two bladed rotor. This resulted in (1) some decrease in  $L/D_{e_{max}}$ , (2) a lower velocity for  $L/D_{e_{max}}$ , (3) a reduction in trim capability, and (4) a slight improvement in  $L/D_e$  at lower velocities. It should be noted that the  $c/D = .027$  for two blades corresponds to a very high value of  $C_T/\sigma$  (0.1745). This is well beyond current design values for conventional rotors and yet still shows reasonable performance for this CCR design.

The previous figures have shown the effect of solidity on rotor performance, the trade-off between  $c/D$  and number of blades to obtain a desirable solidity, and the combined affect of these parameters on rotor cruise efficiency and trim capability. Two rotor configurations were selected from the above consideration for further analysis; a two bladed rotor with  $c/D = .04$ , and a four bladed rotor with  $c/D = .027$ . Airfoil geometry for the two configurations is the same. Definition of rotor designs and airfoil geometry is given in Table 2 and 3 respectively.

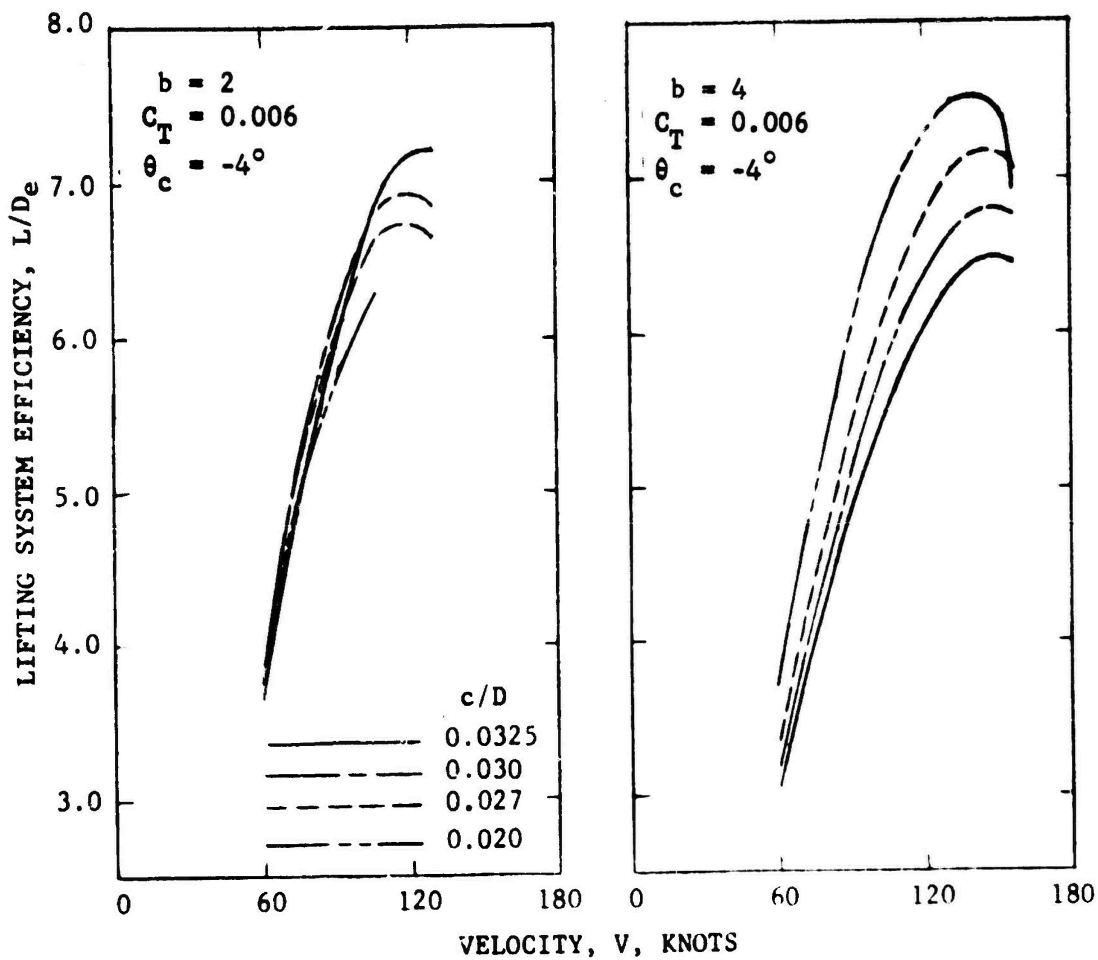


Figure 15 - Typical Solidity Effect on Cruise Performance  
 (Constant Section,  $t/c = 0.20$ ,  $\delta/c = 0.0$ )

TABLE 2 - ROTOR DESIGNS

ROTOR DESIGNS		
Number of blades, b	2	4
Chord/Diameter, c/D	0.04	0.027
Solidity, $\sigma$	0.05092	0.06875
Design Hover Disc Loading, lb/ft <sup>2</sup>	5.22	5.22
Design Tip Speed, fps	600.	550.
Design Hover $C_T/\sigma$	0.12	0.107
Design Twist, deg	-8.63	-8 63

TABLE 3 - AIRFOIL GEOMETRY

AIRFOIL GEOMETRY			
Parameter	Root x = 0.125	Tip x = 1.0	Variation
Thickness Ratio, t/c	0.25	0.15	Linear
Camber, $\delta/c$	0.0625	0.00	Linear
Trailing Edge Radius, r/c	0.05	0.04	Linear
Slot Location, $\bar{x}/c$	0.97	0.97	Constant
Slot Height, h/c	0.001	0.0025	Figure 12

## PERFORMANCE RESULTS

The effects of several design parameters on overall rotor performance were examined for the two rotor configurations of Table 2. Variations of tip speed, blade collective pitch angle, blade twist and taper, and relative disc loading were considered. Hot day performance was also predicted. One of the most significant differences between CCR and conventional rotor performance is the ability of CCR to produce a constant thrust over a finite range of blade collective angle, (i.e., there is not a one to one correspondence between thrust and collective pitch setting). There is however, an optimum collective pitch for a given thrust and flight condition, which is shown later. The parametric variations of tip speed, blade twist and taper, and relative disc loading are shown for a selected collective pitch angle which is not necessarily optimum.

### EFFECT OF TIP SPEED

Tip speed,  $V_T$ , is an important parameter since it impacts on  $C_T/\sigma$ , advance ratio, and compressibility affects simultaneously. An additional higher order affect is a change in the relative importance of lift due to angle of attack and lift due to blowing, which tends to change the radial lift distribution shape. Figure 16 shows the effect of  $V_T$  on hover Figure of Merit (FM) for a range of blade collective pitch settings, and on  $L/D_e$  in forward flight for a specific collective pitch. Reduced tip speed in hover is advantageous for both rotor designs, due primarily to the increase in operating  $C_l$  of the sections. At a forward flight condition however, the trend begins to reverse. The two bladed rotor definitely gives better forward flight performance at  $V_T = 600$  fps. This lower solidity configuration requires a higher tip speed to reduce section  $C_l$  requirements for trim in cruise flight. However, the four bladed rotor operates more efficiently with the lower tip speed up to the trim limit. The sudden efficiency drop off is due primarily to the compressed advance ratio scale corresponding to the lower tip speed. This trim limitation, even though shown for only one collective angle, was considered unacceptable and so a compromised tip speed,  $V_T = 550$  fps, was selected for the four bladed rotor. These respective tip speeds

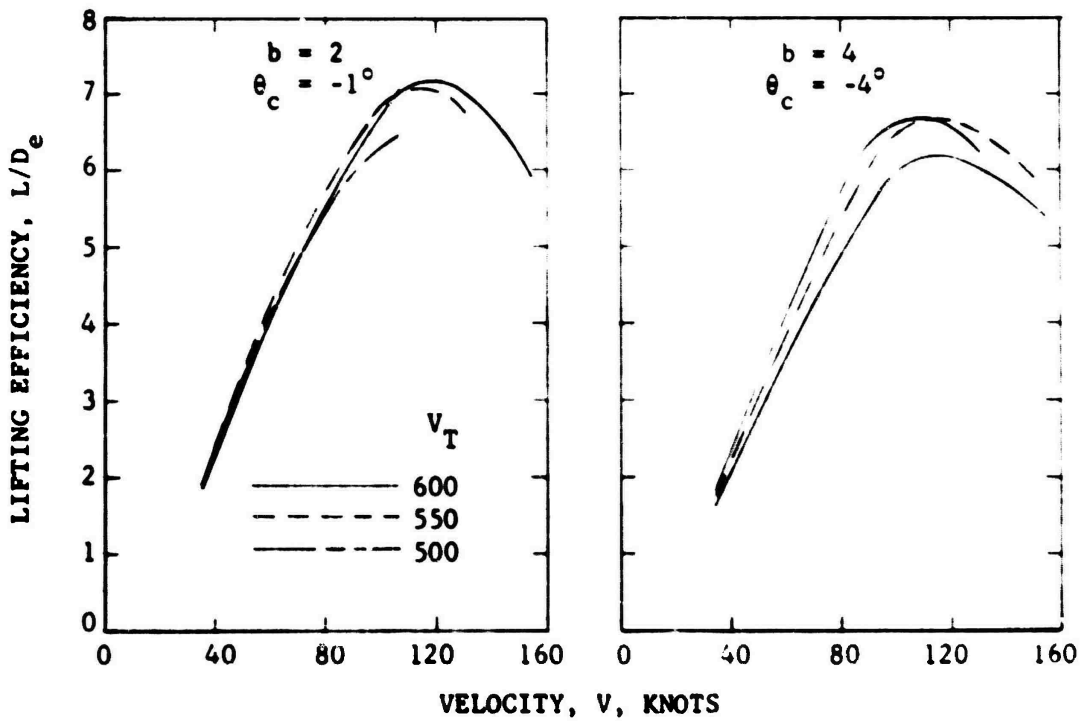
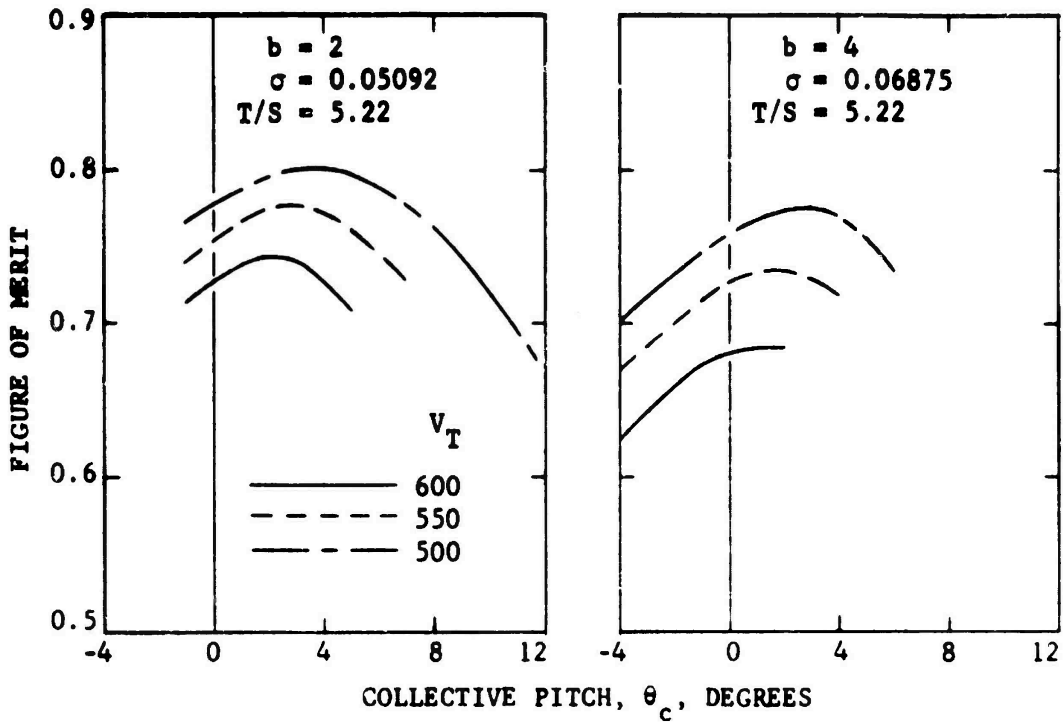


Figure 16 - Tip Speed Effect on Rotor Performance

were used in succeeding performance predictions based on improved forward flight performance. Reduced hover tip speeds would have been preferable if maximum cruise speed requirements had been lower.

#### DISC LOADING AND SOLIDITY

Performance sensitivity to disc loading, or gross weight, variation provides an indication of performance for overload conditions, hot day conditions, and maneuver margin. As this design is based on a constrained hover disc loading with  $C_T/\sigma$ , or tip speed, chosen for cruise flight, other values of disc loading represent off-design conditions in cruise and should reflect decreased performance. This does not suggest that performance could not be as good or better for designs based on other disc loadings. Increased disc loading, or  $C_T/\sigma$ , is beneficial to hover Figure of Merit for both rotor configurations as shown in Figure 17. This pattern was also shown in Figure 16 where decreased tip speed provided higher  $C_T/\sigma$  and improved Figure of Merit. However, cruise selected tip speed places  $C_T/\sigma$  near the optimum for cruise, so effects of disc loading variation on  $L/D_e$  are slightly detrimental. This trend is shown in Figure 17 at a cruise speed of 106.6 knots, indicating that cruise efficiency is relatively insensitive to disc loading variation. This is an important characteristic of CC rotors.

The effect of solidity, or  $c/D$ , on hover efficiency is shown in Figure 18 for the two bladed rotor. Again hover efficiency improves with increased  $C_T/\sigma$ , but solidity also impacts strongly on the compressor power to total power ratio required. As solidity increases, lift due to angle of attack increases requiring significantly lower percentages of compressor power for the same disc loading. Figure 18 also shows this compressor power ratio as it varies with collective pitch angle and  $C_T/\sigma$ . Although compressor power may be reduced for  $C_T/\sigma = .16$  by operation at higher collective angles, comparison to the Figure of Merit curves shows that total power requirements would increase. Compressor power ratio for maximum Figure of Merit is shown to vary from  $\sim 0.02$  at  $C_T/\sigma = .096$  up to  $\sim 0.06$  at  $C_T/\sigma = .16$ . In practice it is unlikely that hover operation would be performed at the optimum combination of collective pitch and collective blowing, but rather at reduced collective angles where the

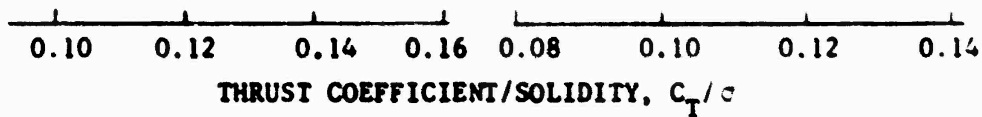
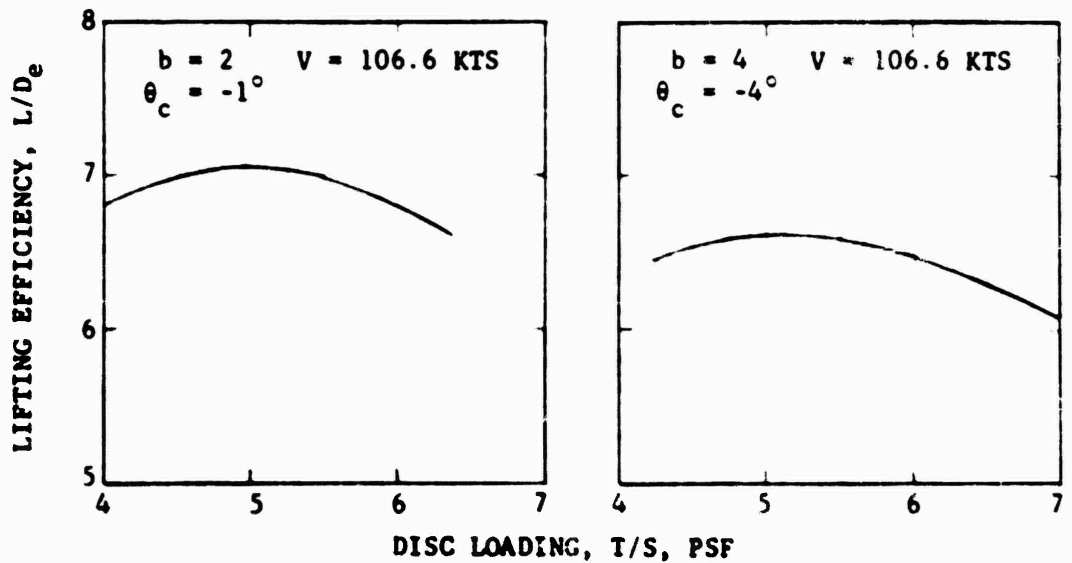
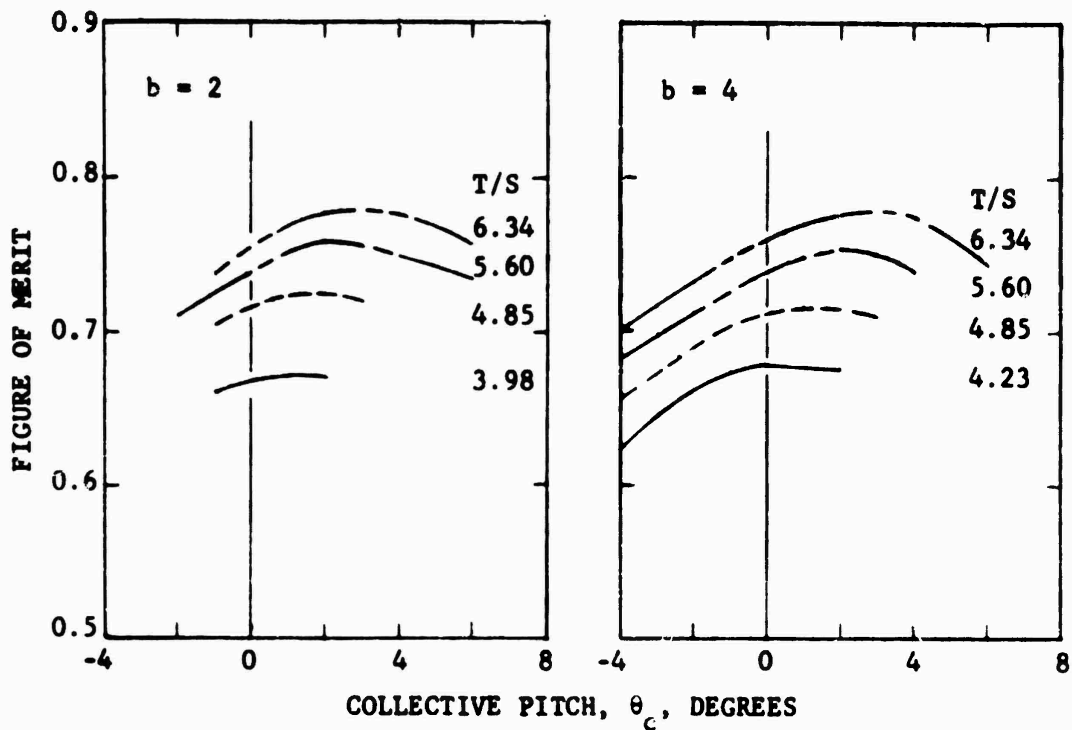


Figure 17 - Disc Loading Effect on Rotor Performance

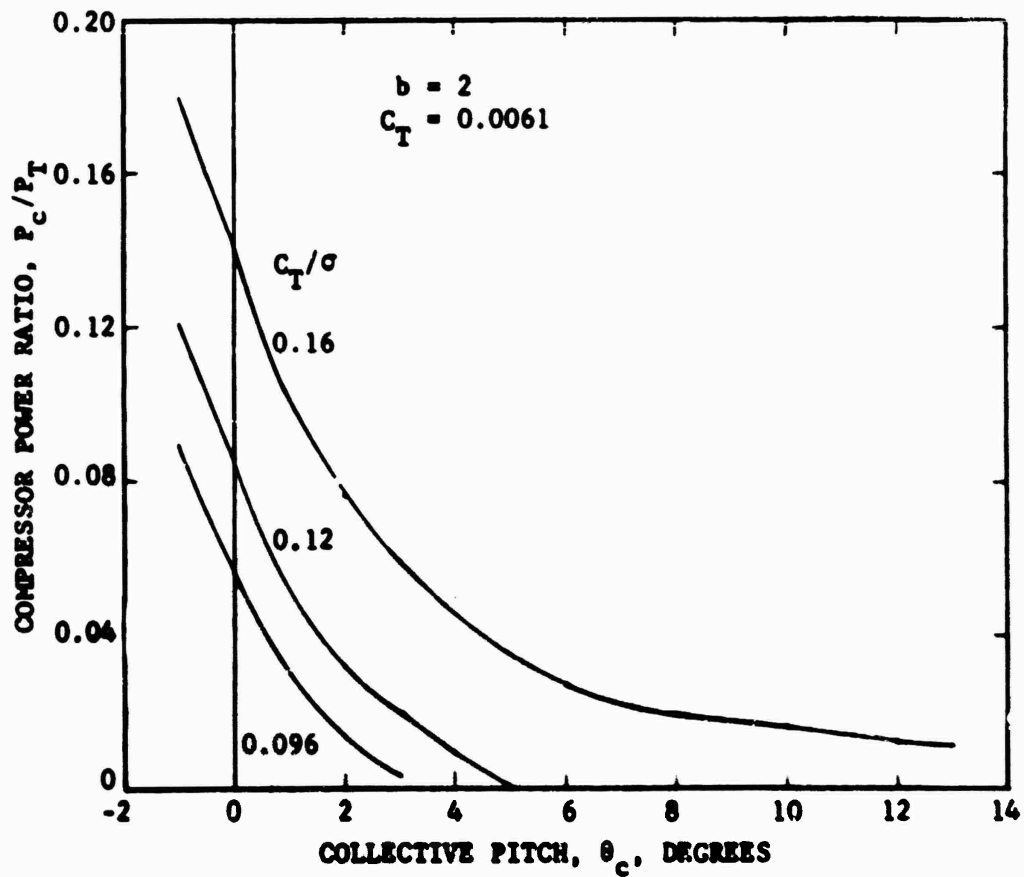
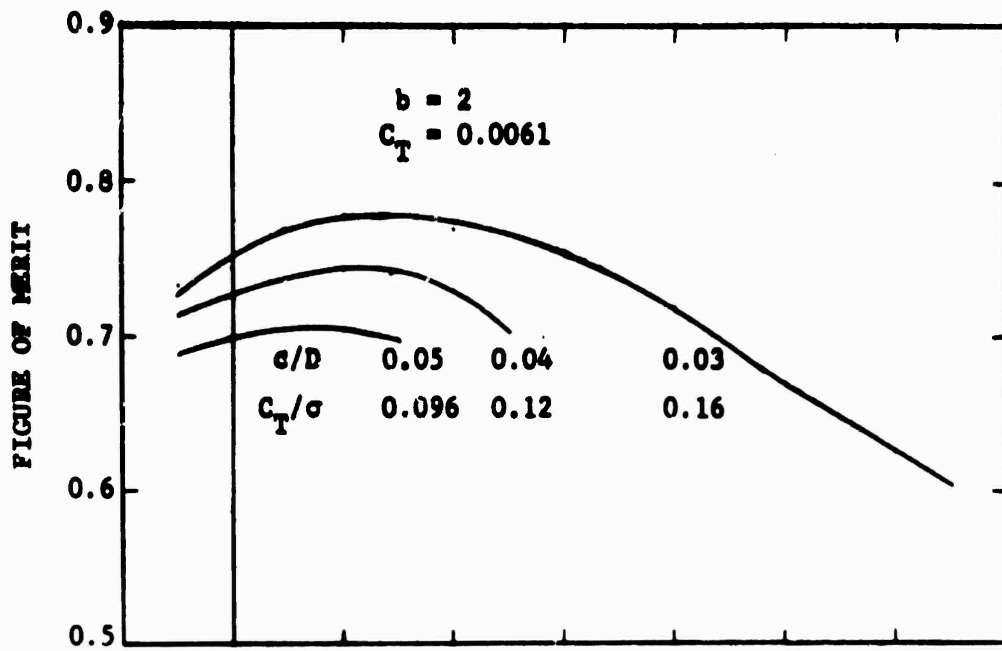


Figure 18 - Solidity Effect on Compressor Power

compressor power ratios are greater. Air compressor size required for a given gross weight vehicle is therefore dependent on the solidity factor. This is an important consideration in vehicle/rotor design from the standpoints of weight and volume, and may well influence the type of air supply used.

#### EFFECT OF TWIST AND TAPER

Twist and taper in conventional rotor designs are used to approach a near uniform inflow in hover, thereby, reducing the all important induced power term. However, in this methodology for CCR design the uniform inflow is approached by proper slot height distribution. This reduces the effect of twist and taper to yielding improvements in section  $L/D_e$  which affects the less important compressor, coriolis, and profile power terms in hover. The effects of twist and taper (for fixed solidity) are shown in Figure 19 for hover and for one advance ratio ( $\mu = 0.3$ ). As noted on the figure these characteristics are for different airfoil geometry than shown in Table 3, but the trends are representative. Maximum hover Figure of Merit is relatively insensitive to twist for the reasons mentioned above, whereas taper is slightly beneficial as it provides more uniform inflow. However, at  $\mu = 0.3$  negative twist yields about 15 percent improvement in  $L/D_e$  compared to no twist and a taper ratio of 0.6 yields about 7 percent improvement in  $L/D_e$  compared to no taper. Increased  $L/D_e$  for the twisted blades is attributed mainly to the associated reduction in compressor power required. At a twist angle of -8.63 degrees the compressor power is only 2/3 of that required for the untwisted blade. This same reduction was found for each of the three taper ratios examined. Compressor power was also found to decrease with increasing taper, but not to an extent that would explain the 7 percent  $L/D_e$  improvement. The exact nature of taper affect on forward flight efficiency is not fully understood at this point.

Twist variations affect the two rotor configurations of Table 2 in the same manner shown in Figure 19, where hover Figure of Merit is essentially unchanged by twist. Cruise  $L/D_e$  sensitivity to twist is shown in Figure 20 for the two rotor designs. The -8.6 degrees of twist gives improved efficiency for both rotors.

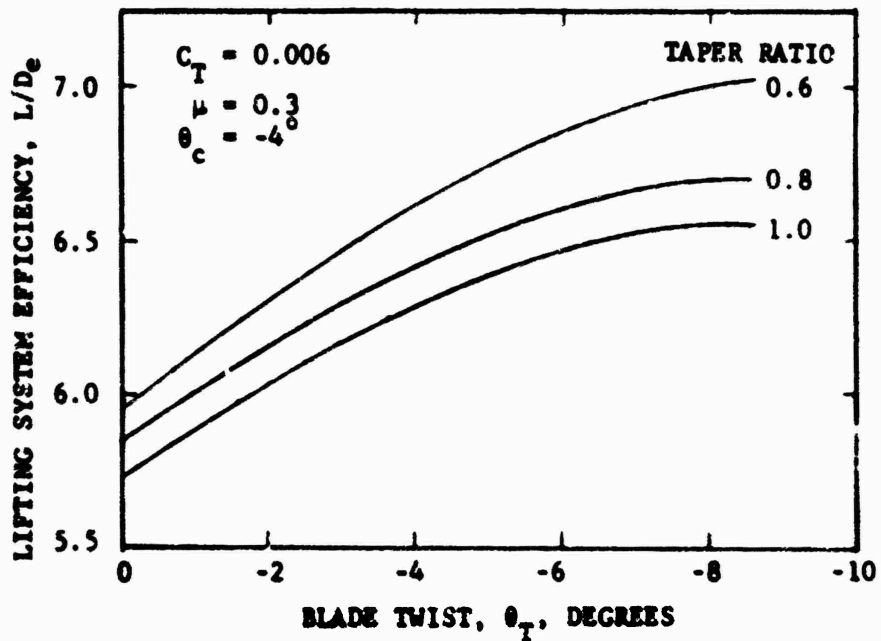
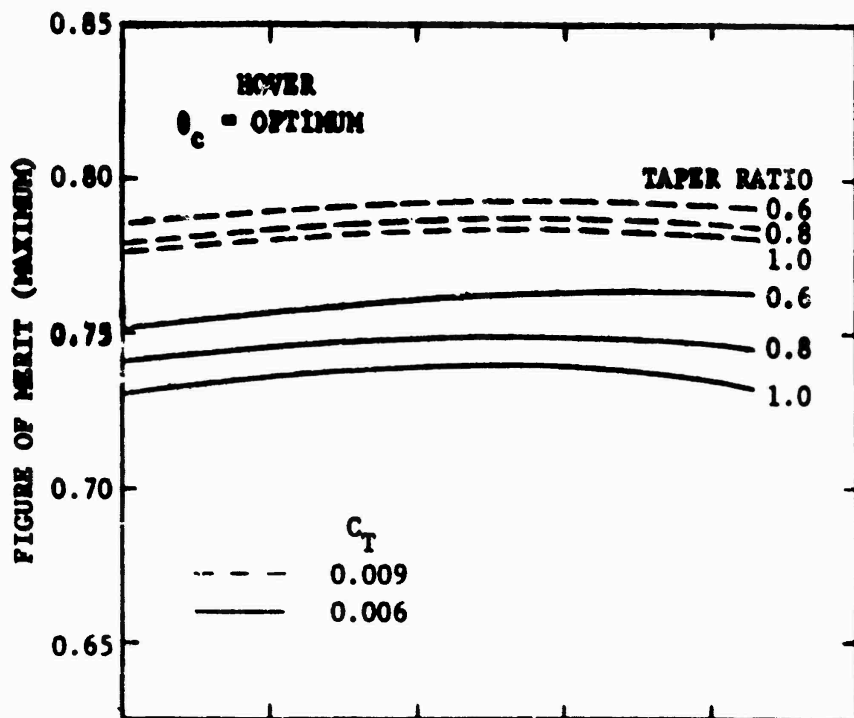


Figure 19 - Typical Effect of Blade Twist and Taper  
 (Constant Section,  $t/c = 0.20$ ,  $\delta/c = 0.0$ )

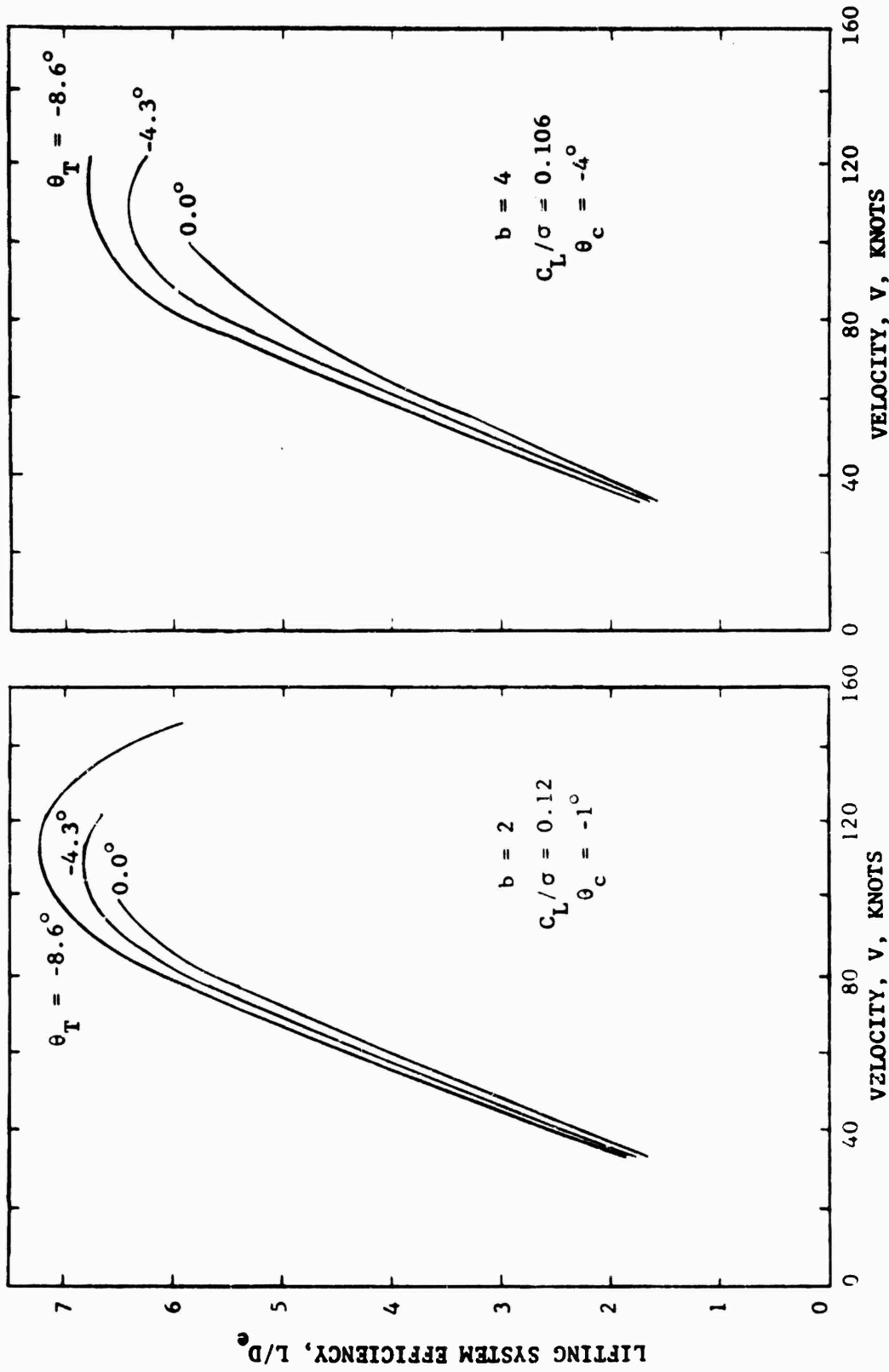


Figure 20 - Effect of Twist on Cruise Efficiency

## HOT DAY PERFORMANCE

As previously noted the disc loading affect of Figure 17 provides an indication of hot day performance. The hot day condition was taken to be  $95^{\circ}$  at a pressure altitude of 5000 feet representing the stringent ARMY requirements. Both hover Figure of Merit and  $C_p/\sigma$  are misleading for hot day performance comparisons due to the density term in their definitions. Where hot day Figure of Merit shows about 7 percent improvement, hot day  $C_p/\sigma$  shows 37 percent more power requirement for the same conditions. Performance comparison is therefore shown in Figure 21 as a direct power ratio, indicating about a 9 percent increase in required power for the hot day hover condition at the same blade collective pitch. Optimum collective pitch angles for each condition show less than a 7 percent difference in minimum powers required for hover.

## POWER COMPONENTS

Compressor power, shaft power, and consequently total power for a given flight condition are dependent on the blade collective pitch setting. Compressor power to total power ratio was shown in Figure 16 to decrease rapidly with increasing collective pitch. Mass flow rate requirements naturally follow compressor power requirements, and are related as follows:

$$C_{P_c} = C_{\dot{w}} \left[ \frac{V_{j_{\max}}}{V_T} \right]^2 \frac{1}{2\eta_c}$$

Power components variation with collective pitch is shown in Figure 22 for the hover case at fixed  $C_T/\sigma$ . Increasing collective pitch requires less compressor power, but more shaft power which is the sum of induced, profile and coriolis contributions. Coriolis power is a function of mass flow rate and so decreases as compressor power decreases. However profile power increases with reduced  $C_l$  or reduced mass flow and the changing radial distribution of  $C_l$  causes corresponding changes in the induced power component. The net effect of these changing power components

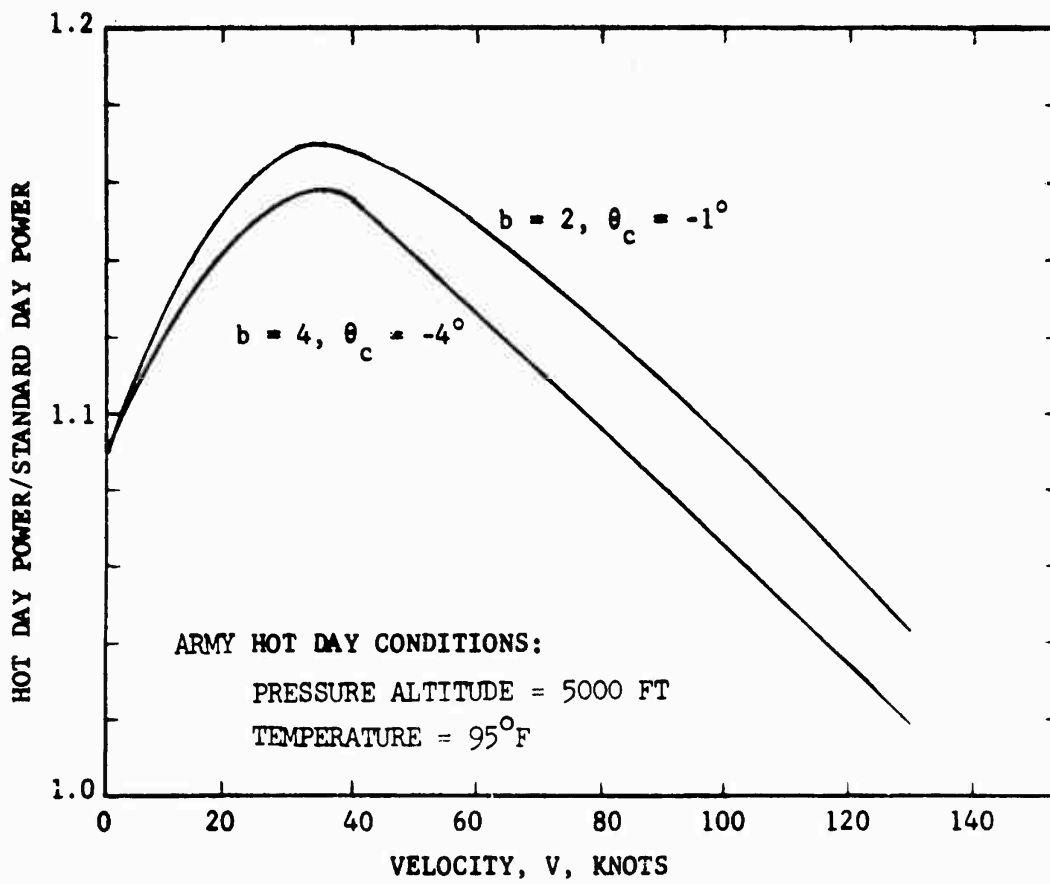


Figure 21 - Hot Day Performance

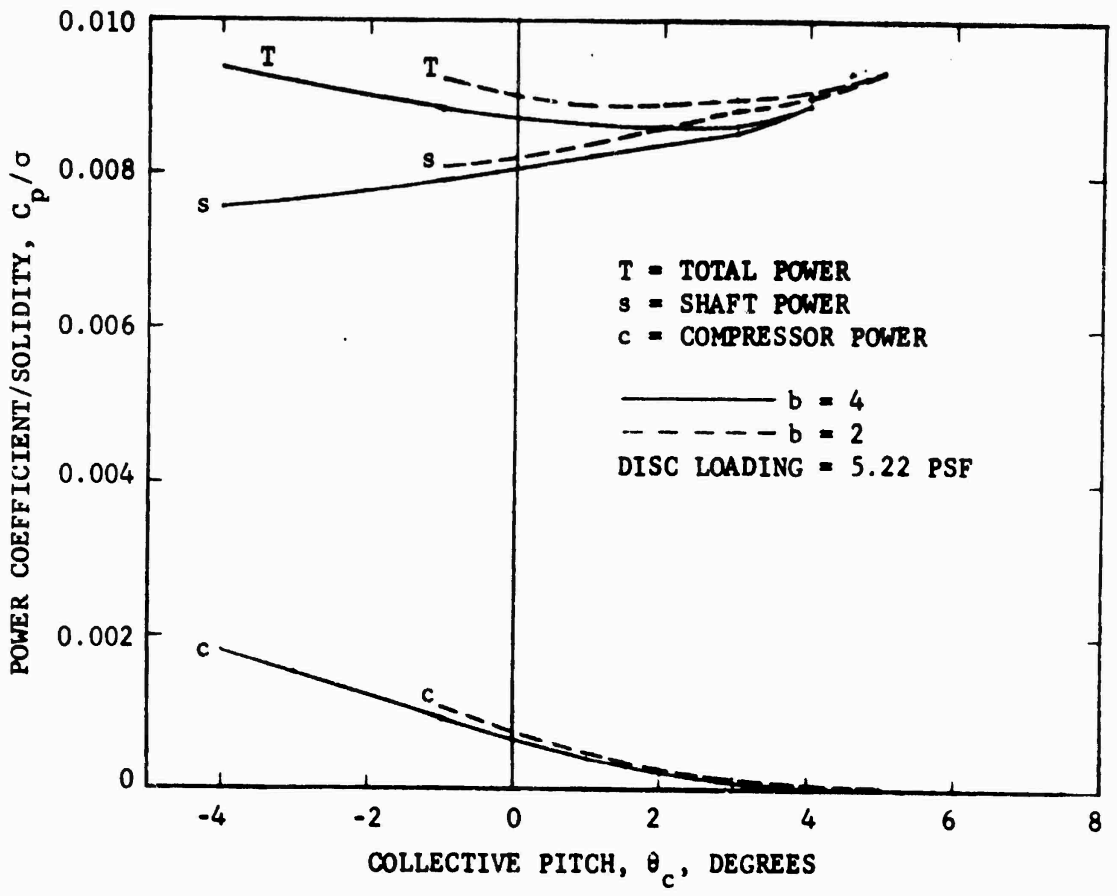


Figure 22 - Hover Power Components Variation with Collective Pitch

is to establish an optimum blade collective pitch, at minimum total power, which requires only a small percentage of compressor power.

Forward flight is compounded by the trim requirement which must be satisfied by the proper variation and magnitude of  $C$ . The mass flow required for trim is a minimum requirement and necessarily increases with speed. This minimum mass flow provides some rotor lift, and the upper limit on collective pitch angle is therefore that value which will provide the remaining lift for a desired thrust. Reduced collective pitch requires application of more collective blowing, or an overall pressure ratio increase superimposed on that required for trim. For the purpose of this study a lower limit on collective pitch is defined when the maximum pressure at any azimuthal position produces a choked condition at the jet exit. Within these limits the operating range of collective pitch is reduced with increased speed, as represented in Figure 23. It is conceivable with this operating range that a practical CCR system could be built with fixed collective pitch. However, autorotation and maneuver capabilities would have to be examined for serious consideration.

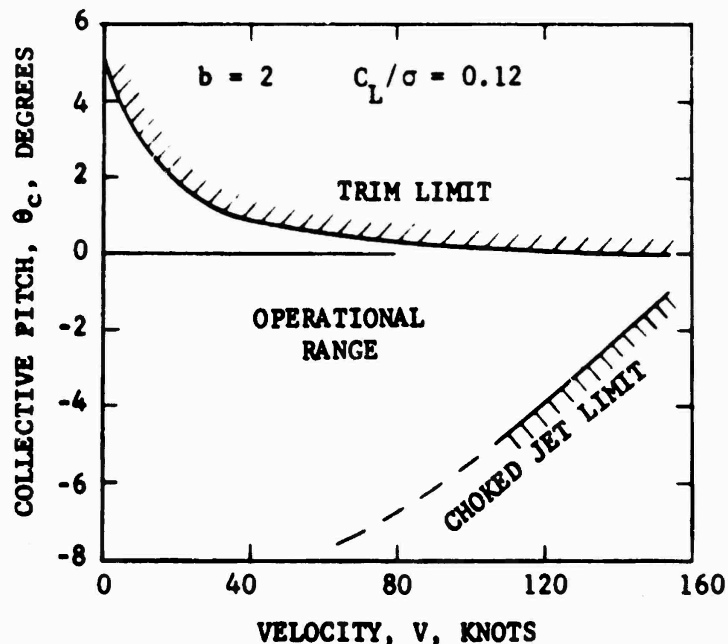


Figure 23 - Typical Limits on Collective Pitch

Variation of rotor total power and compressor power required with  $C_T/\sigma$  is shown in Figure 24 for hover and for 0.3 advance ratio at a fixed collective pitch. Although comparison to Figure 22 shows that the collective pitch angles of Figure 24 are not optimum, the curves do show power sensitivity to  $C_T/\sigma$  and compatible compressor power requirements between hover and forward flight. Figure 25 shows rotor power variation with flight speed for several collective pitch angles. Curves for lower collective pitch angles which terminate at speeds less than 154 knots were limited by the choked jet condition. Non-dimensional mass flow requirements are also shown in Figure 25 for the same flight conditions. As with any rotor design, the curve shapes shown in Figure 25 are very dependent on the operating disc loading and tip speed. The power variation shown represents a design which favored cruise flight efficiency over hovering efficiency. Therefore, comparison to conventional rotor systems of the same disc loading will generally show these CCR power requirements to be somewhat greater in low speed flight, but significantly less at higher velocity. Power requirements for this CCR design may also be reduced for low speed flight, at the expense of cruise flight power, by reducing blade tip speed (increasing  $C_T/\sigma$ ). This simply represents the hover-cruise flight-maneuver compromise required in any rotor design, as previously reflected in Figure 16.

#### MASS FLOW RATES

The required variation of mass flow with azimuthal station for a single blade is shown in Figure 26 for both the two-bladed and the four-bladed rotor configurations. Peak-to-peak amplitude represents that mass flow variation required for trim, whereas the mean amplitude is dependent on the thrust and collective pitch angle combination. As shown in Figure 25 the overall rotor mass flow requirement increases for reduced collective pitch angles. Although not shown, the two rotor designs have nearly equal mass flow requirements as they approach their respective trim limited collective angles (see Figure 23). In the hover condition this is obvious since the trim limit corresponds to zero mass flow for both rotor designs. For the same total mass flow requirement the two-bladed rotor must have twice the mass flow per blade as the four-bladed

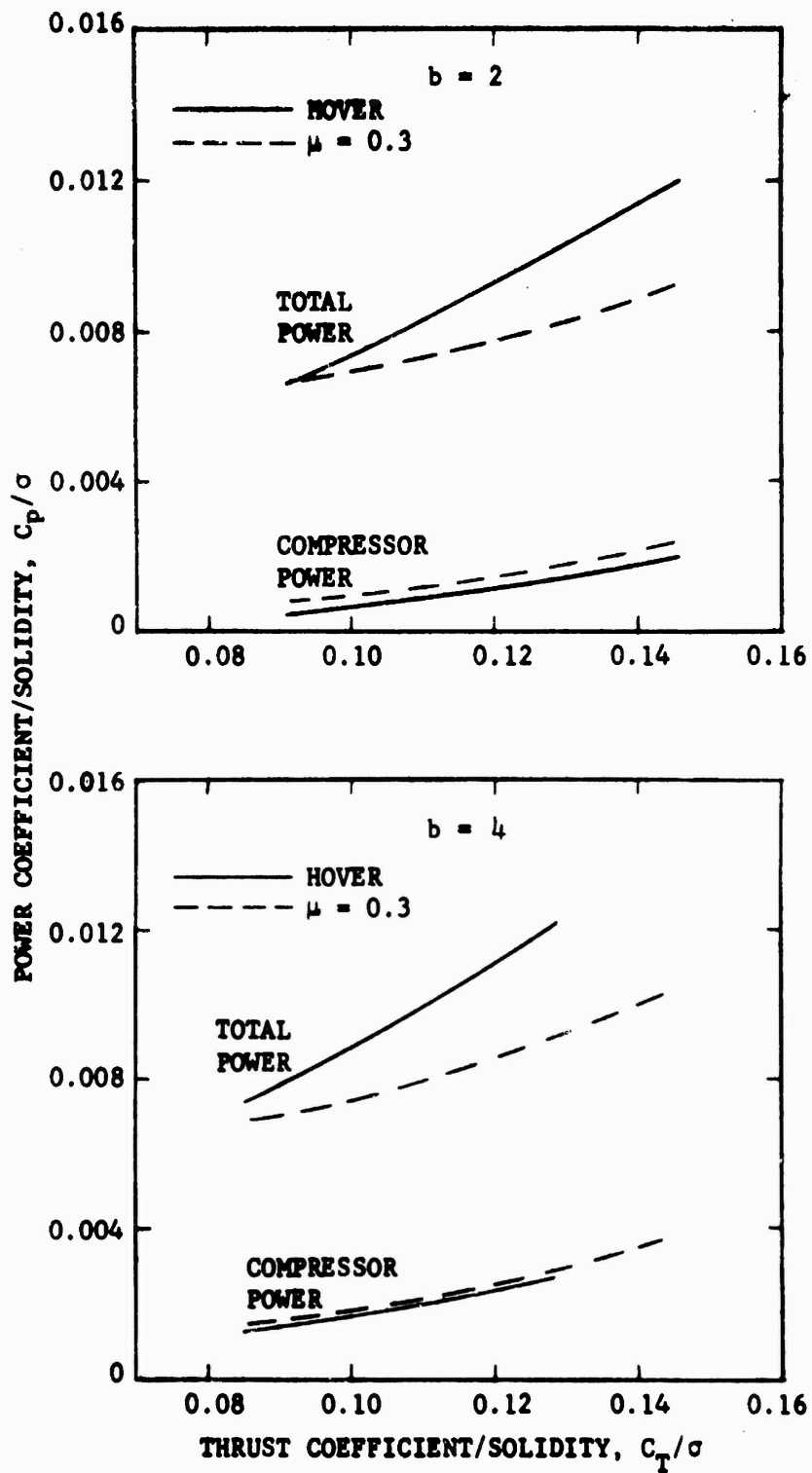


Figure 24 - Power Sensitivity to Thrust Variation

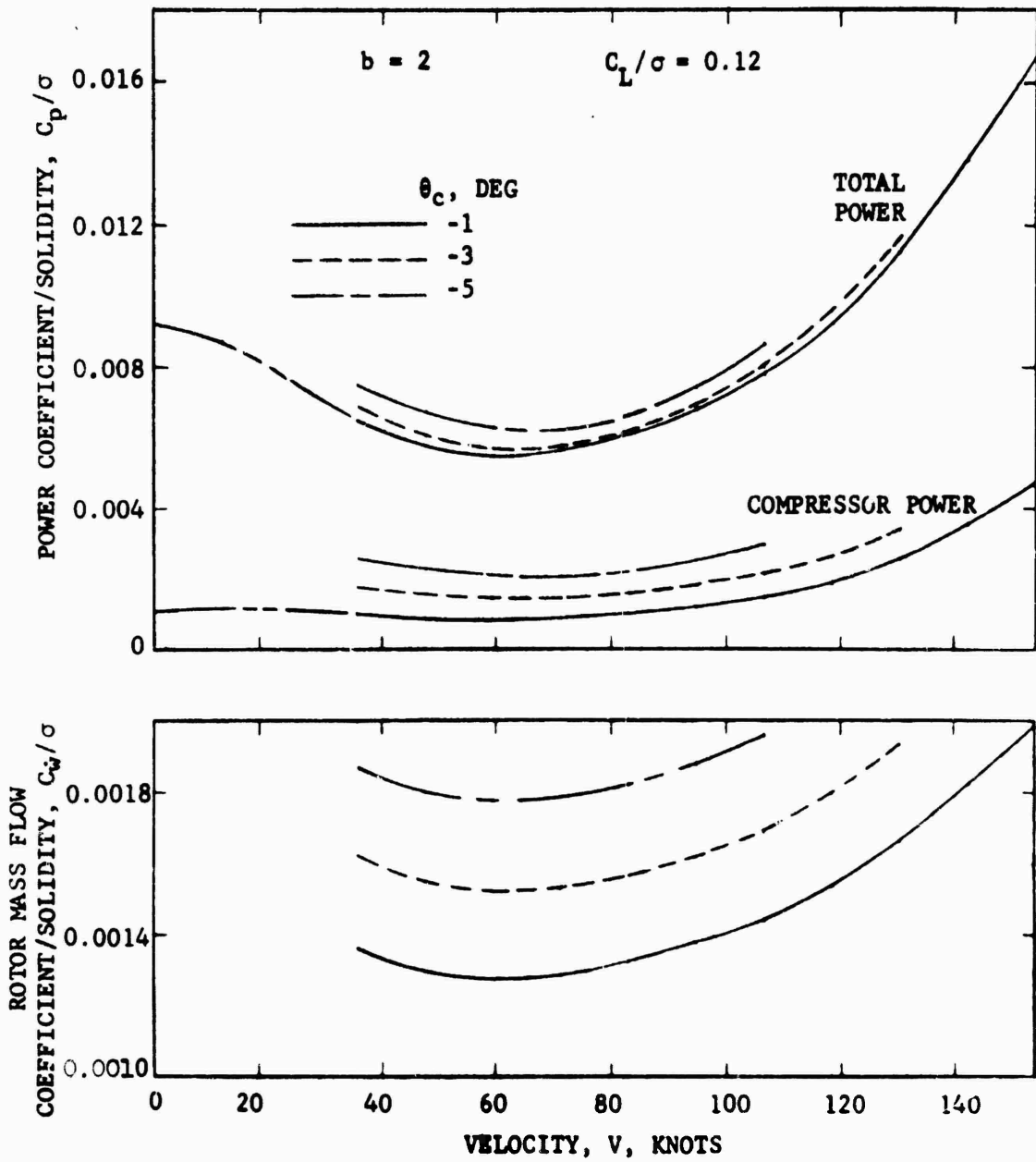


Figure 25a - Two-Bladed Rotor

Figure 25 - Power and Mass Flow Variation with Velocity

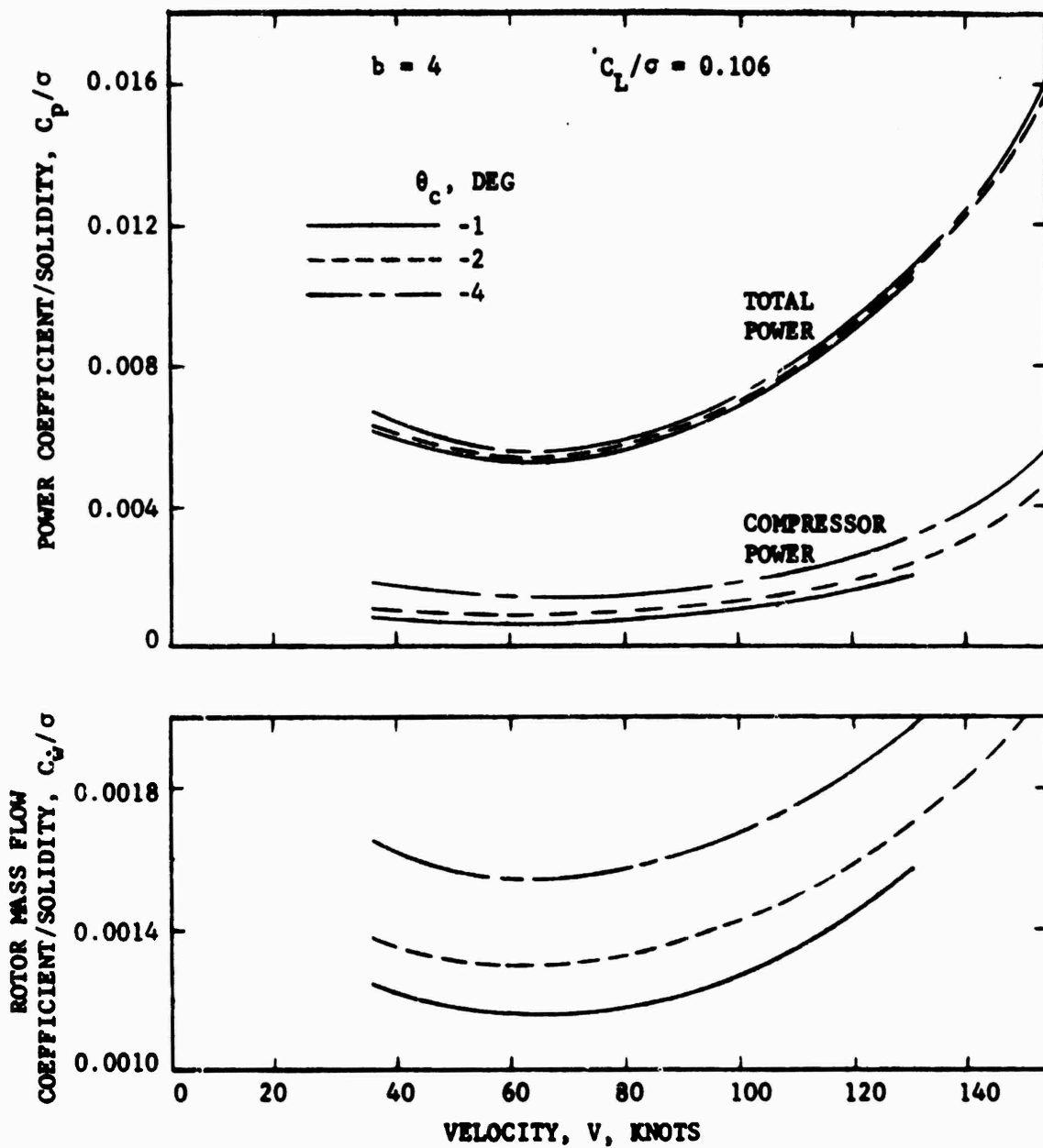


Figure 25b - Four-Bladed Rotor

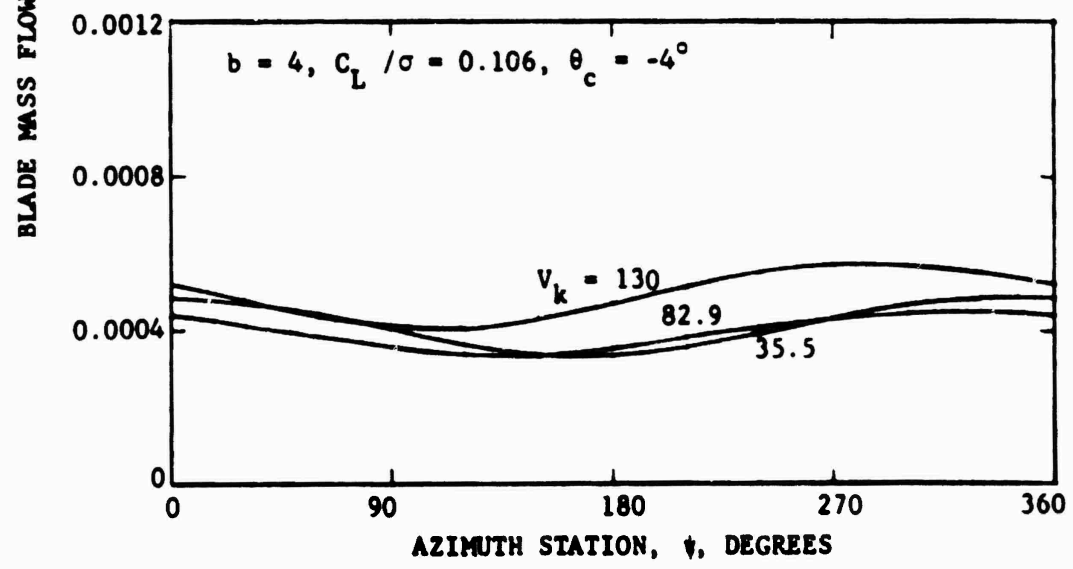
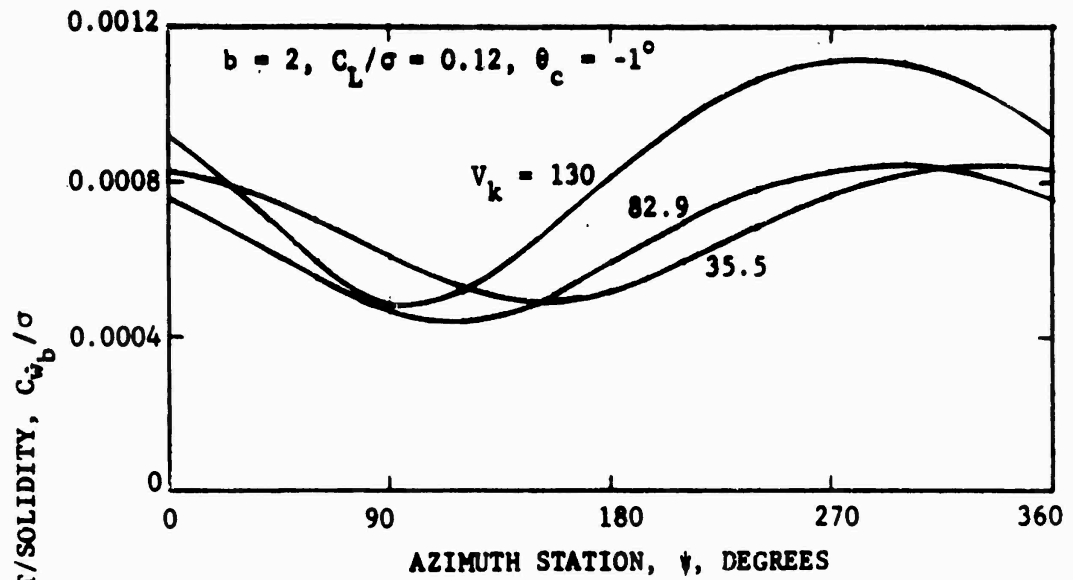


Figure 26 - Typical Blade Mass Flow Variation with Azimuth

rotor. This is verified by the relative mass flow rates per blade shown in Figure 26. The two-bladed rotor also requires a greater peak-to-peak amplitude of mass flow than the four-bladed rotor to satisfy trim requirements. This is a common characteristic of two-bladed rotor configurations and accounts for the source of greater vertical vibration excitation.

Different chord lengths and different blade mass flow rates provide for different duct air and slot air velocities between the two rotor designs. Since both designs have the same  $h/c$  variation, the ratio of their respective slot heights is directly proportional to the ratio of their chord lengths. The ratio of the two rotor designs available internal duct area is proportional to the square of their chord length ratio. Using these geometric relations and the given mass flow rates a simple comparison can be made of the two rotor designs duct air velocity and slot air velocity. Typically the two-bladed rotor would have 9 percent less duct air velocity and only 35 percent greater slot air velocity in comparison to the four-bladed rotor, even with the blade mass flow being twice that of the four-bladed rotor. The lower duct air velocity should decrease duct pressure losses. The greater slot air velocity is aerodynamically more effective, but requires greater duct pressures and consequently increases compressor power. Figure 25 shows the increased compressor power of the two-bladed rotor in comparison to the four-bladed rotor. In making this comparison it should be noted that the power curves for the four-bladed rotor have taken advantage of a reduced tip speed,  $V_T = 550$  fps, which had a strong influence on rotor performance as shown in Figure 16.

#### CONCLUSIONS

This rotor design study, its constraints and parametric trade-offs, yielded the following conclusions:

- A Circulation Control Rotor (CCR), constrained to operate at conventional  $C_T$ , requires reduced solidity to obtain the  $C_T/\sigma$  range for best CCR efficiency. A design without constraints would in general prefer a higher disc loading range.

- The hover-forward flight compromise required a cruise designed  $C_T/\sigma$  which is less than optimum for the hover condition. This produced a rotor system whose efficiency is relatively insensitive to disc loading in cruise flight, and improves with increased disc loading in hover.
- Overall rotor efficiency for the constrained CCR design is still competitive with current conventional helicopters. Hover Figure of Merit for the CCR design approaches 0.8 with reduced tip speed, and cruise efficiency ( $L/D_e$ ) exceeds 7.0 in the propulsive mode.
- The CCR can operate over a wide range of blade collective pitch angles while generating a set thrust. This collective angle range has a definite upper limit established by trim requirements, and a lower limit established by the choked jet condition. Operation is possible beyond the choked jet condition but is relatively inefficient. Within these limits the collective angle range narrows with increasing velocity. The optimum collective angle is generally one or two degrees less than the established upper limit.
- Shaft power, and thus shaft torque for a given RPM, can be less for the CCR design than for conventional rotor systems. This would reduce tail rotor anti-torque power in proportion to the quantity of main rotor blowing. The significance of this anti-torque power reduction has not been addressed, but should be evaluated.
- Geometric blade twist is beneficial for the CCR design for moderate forward flight speeds. Minimum induced power thru proper slot height distribution eliminates any significant affect of twist in the hover and low speed flight conditions.

#### ACKNOWLEDGEMENT

The author would like to express appreciation to Mr. Robert J. Englar for his procedure and valuable assistance in the airfoil trailing edge radius and slot location design; Mr. Drew Wm. Linck for contributions in developing and refining the computer program; Mr. Stephen Baker for assistance in the study; and Mr. Philip Dodd for assistance in the early test/theory correlation.

## Appendix A

### BASIC SECTION DATA

Basic two-dimensional airfoil data is available over a wide range of  $C_{\mu}$  and  $\nu$  in References 2 thru 5. Section data representation in the performance programs is by a three dimensional table look-up consisting of  $(\alpha, C_l, \text{ and } C_d)$  for each of three basic airfoil thickness ratios,  $t/c = 0.30, 0.20, 0.15$ . Computer plots of this data are shown in Figure A1 and A2 for  $t/c = 0.30$  and  $t/c = 0.15$  respectively. Data for  $t/c = 0.20$  may be found in References 2 and 10. Each section differs not only in  $t/c$ , but also in the  $h/c, \delta/c, r_{te}/c$ , and the reference Reynolds number. This was taken into account through the section data refinements of Appendix B, which were obtained from additional two-dimensional data on the same airfoil models.

These refinements then allow accurate representation of section characteristics over a broader range of conditions than the basic data. Section characteristics for intermediate airfoil thickness ratios along the blade span were obtained by a quadratic interpolation using the three sets of basic airfoil data.

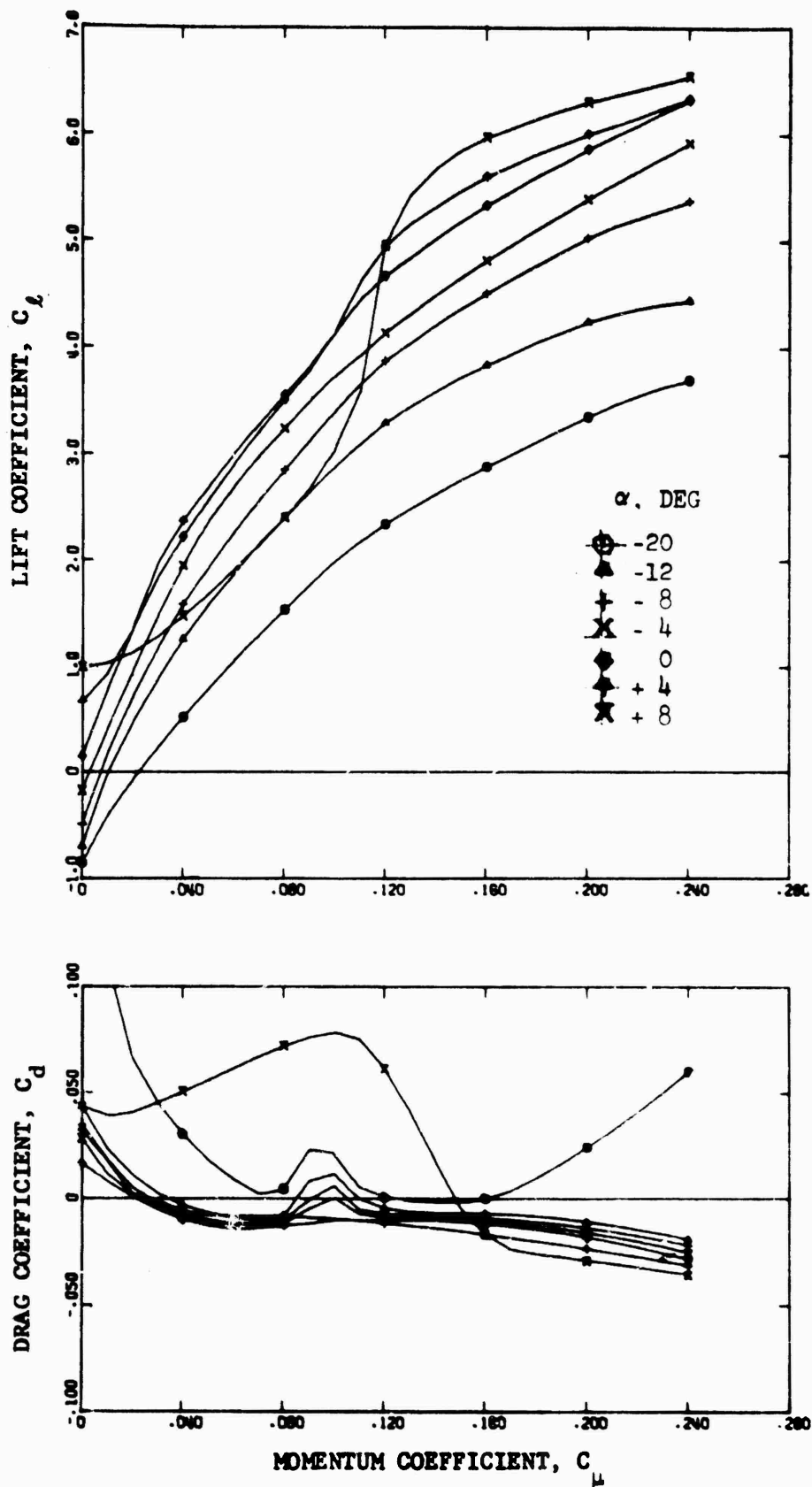


Figure A.1 - Circulation Control Airfoil Data  
 (Ref. 5:  $t/c = 0.30$ ,  $\delta/c = 0.015$ ,  $h/c = 0.00167$ )

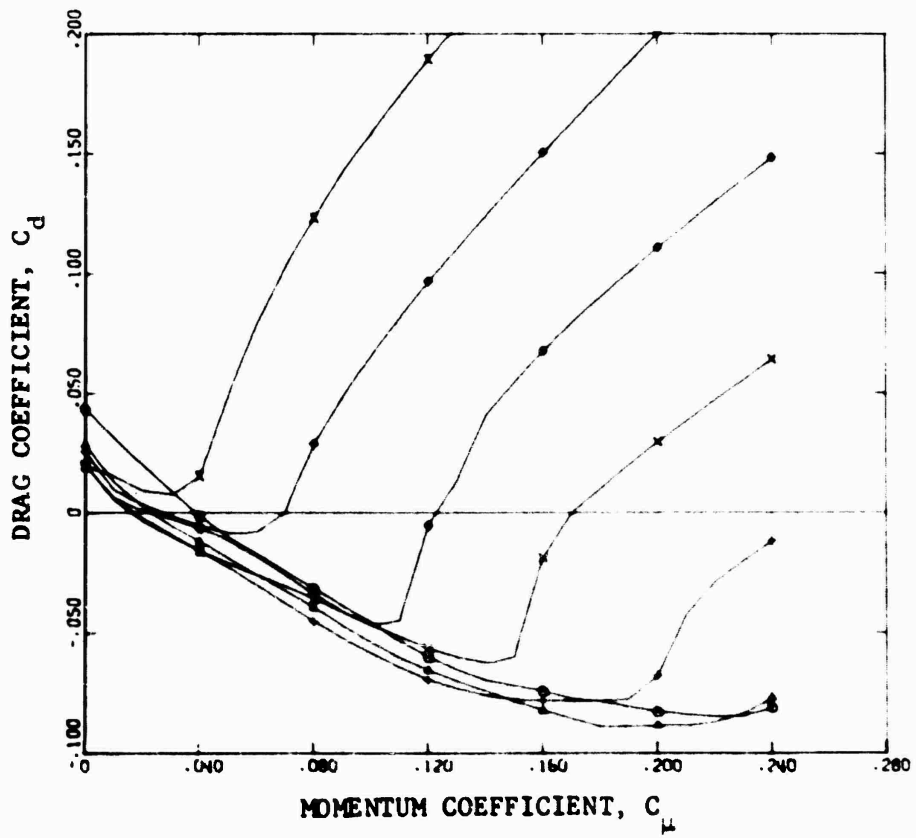
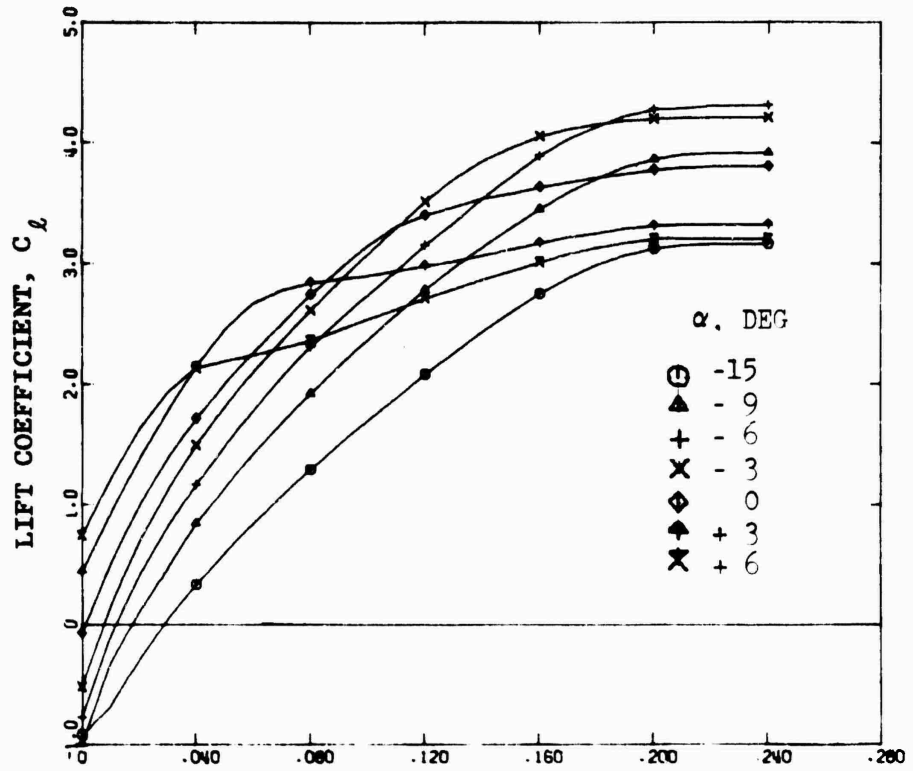


Figure A.2 - Circulation Control Airfoil Data  
 (Ref. 4;  $t/c = 0.15$ ,  $\delta/c = 0.0$ ,  $h/c = 0.0013$ )

## APPENDIX B

### SECTION DATA REFINEMENTS

#### Camber

Airfoil camber changes were considered to affect a uniform translation in the  $C_l - C_{lu}$  and  $C_d - C_{ld}$  curves. This was based on  $C_l$  and  $C_d$  values obtained from various cambered 2-D models at zero angle of attack with no blowing. The effect of camber on  $C_l$  and  $C_d$  is shown in Figure B1. A reduction in camber from basic data for instance was accomplished by first adjusting camber to zero, and then adding back in the  $\Delta$  corrections required.

#### Reynolds Number

Tabulated basic data was for a specific Reynolds number, but the rotor blade airfoil sections operate over a wide range of Reynolds numbers. Additional two-dimensional data provided a correction for the low range of Reynolds number as shown in Figure B2. The correction was applied in the form of an effective  $C_{lu}$ , which is less than actual  $C_{lu}$  for Reynolds numbers less than that of the basic section data. This effective  $C_{lu}$  was then used in the table look-up routine to determine the  $C_l$  and  $C_d$  values appropriate to the operating Reynolds numbers. Actual  $C_{lu}$  and actual mass flow were retained for calculation of compressor power and rotor mass flow requirements.

#### Slot Height-to-Chord Ratio

Distributed slot height in the radial direction, to yield minimum induced power, required slot height-to-chord ratios ( $h/c$ ) different from the basic data. Additional 2-D data for various slot heights gave the  $h/c$  refinement of Figure B3. This refinement for section  $C_l$  was applied last as a direct  $C_l$  (corrected)/ $C_l$  (basic data) ratio. The curves show decreased lift augmentation (reduced  $C_l$  at constant  $C_{lu}$ ) for increasing slot height-to-chord ratios beyond the basic data. These refinements were found to hold over a wide range of angle of attack, and so were applied over the entire operational range seen by the section. The effective  $C_{lu}$  from the Reynolds number correction was used to determine the corrected  $C_l$  in Figure B3, thereby amplifying the effects of each.

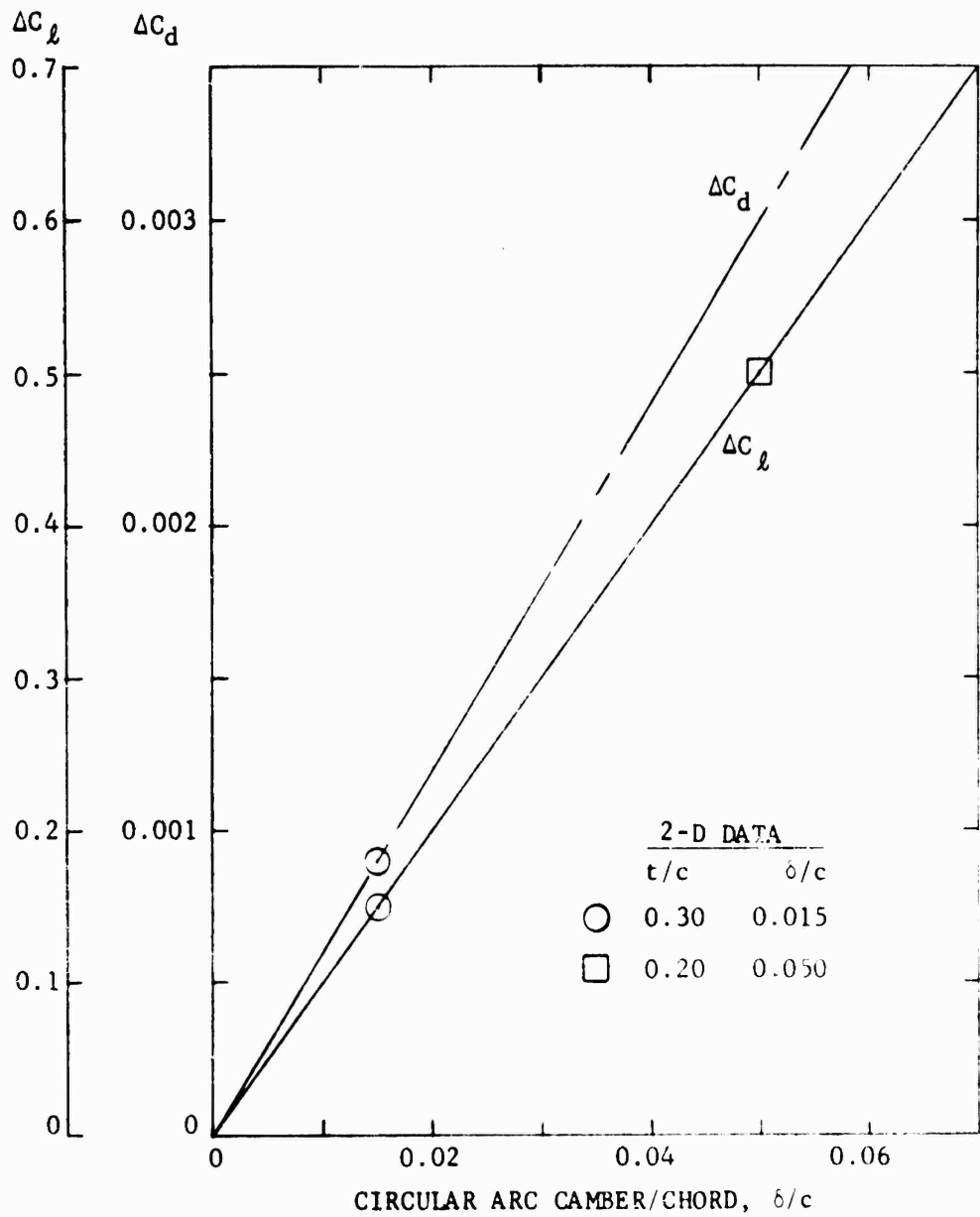


Figure B.1 - - Section Data Camber Refinement

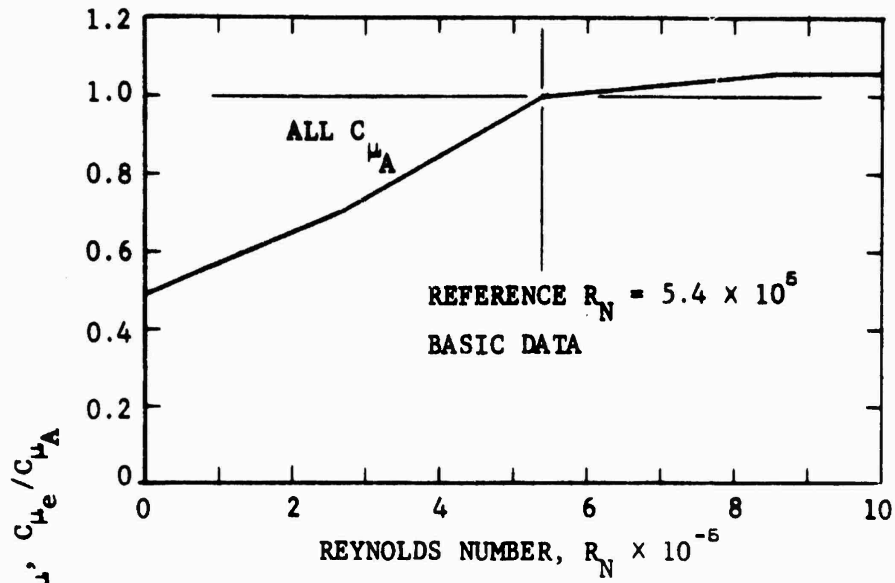


Figure B.2a -  $t/c = 0.15$ ,  $\delta/c = 0.0$ ,  $h/c = 0.0013$

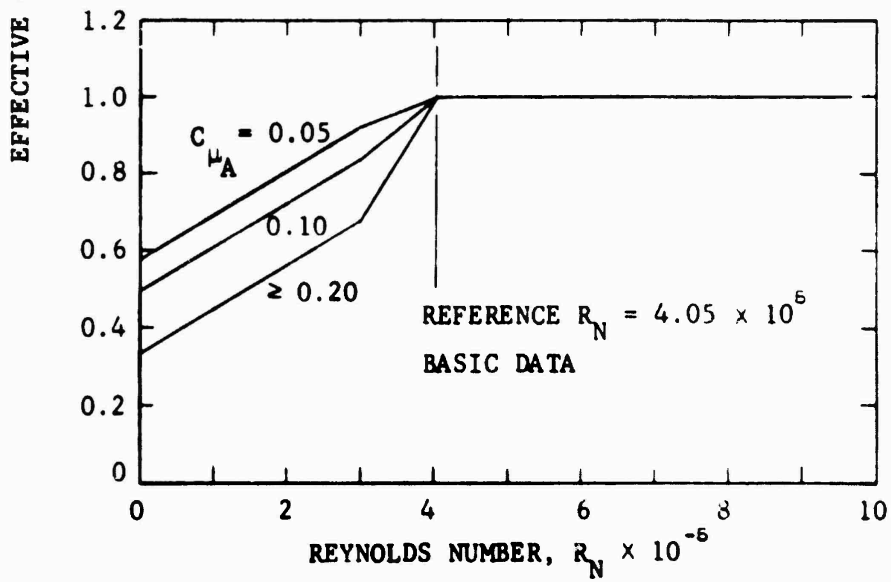


Figure B.2b -  $t/c = 0.30$ ,  $\delta/c = 0.015$ ,  $h/c = 0.00167$

Figure B.2 - Reynolds Number Correction

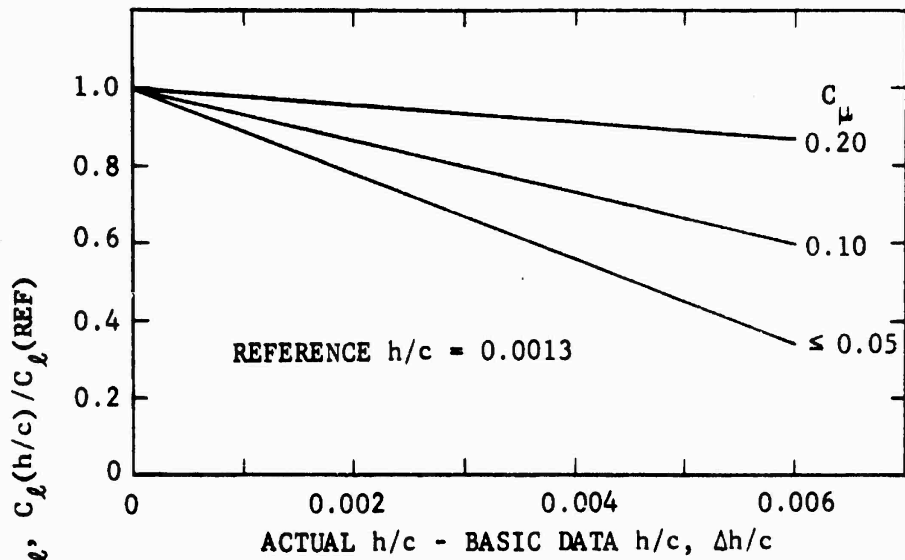


Figure B.3a -  $t/c = 0.15$ ,  $\delta/c = 0.0$ ,  $R_N = 5.4 \times 10^5$

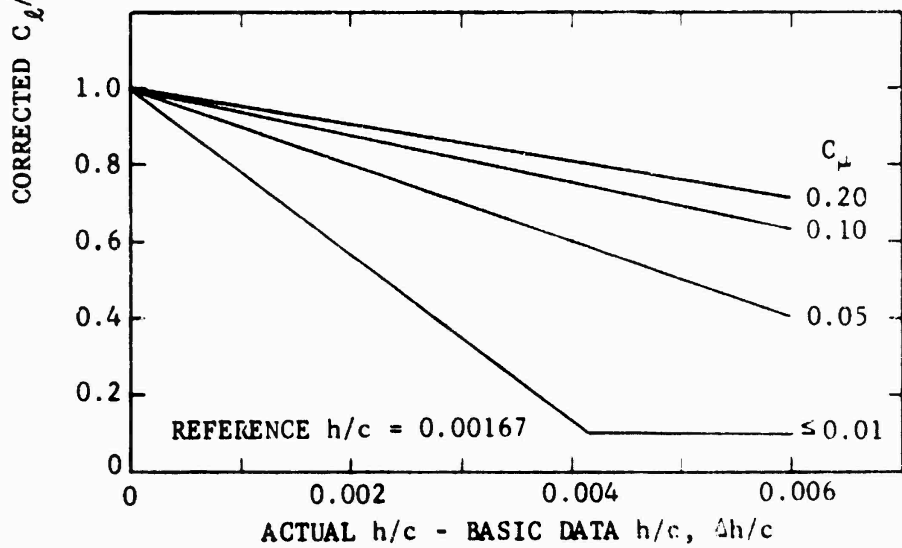


Figure B.3b -  $t/c = 0.30$ ,  $\delta/c = 0.15$ ,  $R_N = 4.05 \times 10^5$

Figure B.3 - Slot Height-to-Chord Refinement

#### REFERENCES

1. Williams, Robert M. "Some Research on Rotor Circulation Control". CAL/AVLABS Symposium: "Aerodynamics of Rotary Wing and V/STOL Aircraft." 3rd, Buffalo, Jan. 1969. Proceedings, Vol. 2.
2. Williams, Robert M. and Harvey J. Howe. "Two Dimensional Subsonic Wind Tunnel Tests on a 20 Percent Thick, 5 Percent Cambered Circulation Control Airfoil". Aug 1970. Naval Ship Research and Development Center Technical Note AL-176. (AD 877-764)
3. Englar, Robert J. "Two-Dimensional Transonic Wind Tunnel Tests of Three 15 Percent Thick Circulation Control Airfoils". Dec 1970. Naval Ship Research and Development Center Technical Note AL-182.
4. Englar, Robert J. "Two-Dimensional Subsonic Wind Tunnel Tests of Two 15-Percent Thick Circulation Control Airfoils", Aug 1971. Naval Ship Research and Development Center Technical Note AL-211.
5. Englar, Robert J. "Two-Dimensional Subsonic Wind Tunnel Tests on a Cambered 30-Percent Thick Circulation Control Airfoil", May 1972. Naval Ship Research and Development Center Technical Note AL-201.
6. Englar, Robert J. "Test Techniques for High Lift Two-Dimensional Airfoils with Boundary Layer and Circulation Control for Application to Rotary Wing Aircraft". Paper presented at Canadian Aeronautics and Space Institute Symposium: "Practical Aspects of V/STOL Wind Tunnel Testing". May 1972. (NSRDC preprint).
7. Rogers, Ernest O. "Critical Mach Numbers of Circulation Control Airfoils as Determined by Finite-Difference Methods", Aug 1972. Naval Ship Research and Development Center Technical Note AL-273.
8. Reader, Kenneth R. "Evaluation of a Pneumatic Valving System for Application to a Circulation Control Rotor", Mar 1973. Naval Ship Research and Development Center Formal Report 4070.
9. Williams, Robert M. and R. A. Hemmerly. "Determination of the (Ideal Practical) Hover Efficiency of Circulation Control Rotors", Aug 1971. Naval Ship Research and Development Center Technical Note AL-212.
10. Williams, Robert M. "Analysis of the Hover Performance of a High Speed Circulation Control Rotor", Aug 1971. Naval Ship Research and Development Center Technical Note AL-221.

11. Williams, Robert M. and E. O. Rogers, "Design Considerations of Circulation Control Rotors". Paper number 603, 28th National Forum of the American Helicopter Society, Wash., D. C., May 1972.
12. Wilkerson, Joseph B., K. R. Reader, and D. W. Linck. "The Application of Circulation Control Aerodynamics to a Helicopter Rotor Model". Paper number 704, 29th National Forum of the American Helicopter Society, Wash., D. C., May 1973.
13. Swihart, John M. "Experimental and Calculated Static Characteristics of a Two-Blade NACA 10-(3) (062)-045 Propeller", NACA RM L54A19, Mar 1954.
14. Englar, Robert J. and Robert M. Williams. "Design of a Circulation Control Stern Plane for Submarine Applications". Mar 1971, Naval Ship Research and Development Center Technical Note AL-200.

## DOCUMENT CONTROL DATA - R &amp; D

(Security classification of title, body of abstract and indexing annotation must be entered when the overall report is classified)

1. ORIGINATING ACTIVITY (Corporate author) Aviation and Surface Effect Department Naval Ship Research and Development Center Bethesda, Maryland 20034		2a. REPORT SECURITY CLASSIFICATION Unclassified	
		2b. GROUP	
3. REPORT TITLE DESIGN AND PERFORMANCE ANALYSIS OF A PROTOTYPE CIRCULATION CONTROL HELICOPTER ROTOR			
4. DESCRIPTIVE NOTES (Type of report and inclusive dates) Technical Note			
5. AUTHOR(S) (First name, middle initial, last name) Joseph B. Wilkerson			
6. REPORT DATE March 1973		7a. TOTAL NO. OF PAGES 60	7b. NO. OF REFS 14
8a. CONTRACT OR GRANT NO.		8b. ORIGINATOR'S REPORT NUMBER(S) Technical Note AL-290	
8c. PROJECT NO. F41.421.210		8d. OTHER REPORT NO(S) (Any other numbers that may be assigned this report)	
8e. NSRDC 1-1690-100			
10. DISTRIBUTION STATEMENT Distribution limited to U. S. Government agencies only; Test and Evaluation; March 1973. Other requests for this document must be referred to Head, Aviation and Surface Effects Department.			
11. SUPPLEMENTARY NOTES		12. SPONSORING MILITARY ACTIVITY Naval Air Systems Command (320)	
13. ABSTRACT A Circulation Control Rotor (CCR) has been designed for application to existing conventional speed helicopters of the 5000 to 10000 pound weight class. A design methodology is shown which tends to minimize rotor induced power in hover while operating at near maximum airfoil section efficiency. The particular design was constrained by conventional disc loadings and blade tip speeds to be consistent with available helicopter engine/transmission combinations. The design is near optimum within these constraints and current available data. Circulation control airfoil and slot geometry design considerations are shown. Tip speed, solidity and disc loading were varied to show performance sensitivity to those parameters and to define the conditions of best overall rotor aerodynamic efficiency. The constrained CCR design was found to operate best at a thrust coefficient/solidity ratio around 0.12. At this condition hover Figure of Merit improved with increased disc loading, while cruise aerodynamic efficiency was relatively insensitive to disc loading changes. Overall performance exceeded or was equal to that of conventional rotor systems for the same weight class vehicle.			

KEY WORDS	LINK A		LINK B		LINK C	
	ROLE	WT	ROLE	WT	ROLE	WT
Boundary Layer Control						
Circulation Control Rotor						
Helicopter Rotor						
High Lift Systems						
Lift Augmentation						